Susceptibility and dilution effects of the kagomé bilayer geometrically frustrated network: A Ga NMR study of $SrCr_{9p}Ga_{12-9p}O_{19}$

L. Limot* and P. Mendels
Laboratoire de Physique des Solides, UMR 8502, Université Paris-Sud, F-91405 Orsay, France

G. Collin
Laboratoire Léon Brillouin, CE Saclay, CEA-CNRS, F-91191 Gif-sur-Yvette, France

C. Mondelli, B. Ouladdiaf, and H. Mutka
Institut Laue-Langevin, B.P. 156, F-38042 Grenoble Cedex 9, France

N. Blanchard
Laboratoire de Physique des Solides, UMR 8502, Université Paris-Sud, F-91405 Orsay, France

M. Mekata
Department of Applied Physics, Fukui University, Fukui 910, Japan
(Received 19 November 2001; published 4 April 2002)

The archetype of geometrically frustrated compounds $SrCr_{9p}Ga_{12-9p}O_{19}$ is a kagomé bilayer of Heisenberg Cr^{3+} ions ($S=3/2$) with antiferromagnetic interactions. We present an extensive gallium nuclear magnetic resonance (NMR) study over a broad Cr-concentration range ($0.72 \leqslant p \leqslant 0.95$). This allows us to probe locally the susceptibility of the kagomé bilayer and separate the intrinsic properties due to geometric frustration from those related to site dilution. Compared to the partial study on one sample, $p=0.90$, presented in Phys. Rev. Lett. **85**, 3496 (2000), we perform here a refined study of the evolution of all the magnetic properties with dilution, with a great emphasis on the lowest diluted $p=0.95$ sample synthesized for this study. Our major findings are the following (1) The intrinsic kagomé bilayer susceptibility reaches a maximum at a temperature of $\approx 40-50$ K, which we show here to be robust up to a dilution as high as $\approx 20\%$; this maximum is the signature of the development of short-range antiferromagnetic correlations in the kagomé bilayer. (2) At low T, a highly dynamical state induces a strong wipeout of the NMR intensity, regardless of dilution. (3) The low-T upturn of the macroscopic susceptibility is associated with paramagnetic defects, which stem from the dilution of the kagomé bilayer. The low-T analysis of the $p=0.95$ NMR line shape, coupled with a more accurate determination of the nuclear Hamiltonian at high T, allows us to discuss in detail the nature of the defect. Our analysis suggests that the defect can be associated with a staggered spin response to the vacancies of the kagomé bilayer. This, altogether with the maximum in the kagomé bilayer susceptibility, is very similar to what is observed in most low-dimensional antiferromagnetic correlated systems, even those with a short spin-spin correlation length. (4) The spin-glass-like freezing observed at $T_g \approx 2-4$ K is not driven by the dilution-induced defects.

DOI: 10.1103/PhysRevB.65.144447 PACS number(s): 75.30.Cr, 75.50.Lk, 76.60.−k

I. INTRODUCTION

Under certain circumstances, it is impossible for magnetic systems to minimize simultaneously all the interactions between the spins. The system is then frustrated. This is known to occur in the spin-glass (SG) compounds where the disorder on the magnetic network induces a competition between the interactions. In a vast variety of systems, the frustration can arise from the geometry of the lattice itself, without disorder,[1] as in the case of the triangular-based antiferromagnetic (AF) networks. The kagomé ($d=2$) and the pyrochlore ($d=3$) networks with AF interactions are a particular class of geometrically frustrated networks where the triangles (for the kagomé lattice) and the tetrahedras (for the pyrochlore lattice) share corners instead of sides as for the familiar triangular network.

Within a classical theory, the ground state is built on triangles and/or tetrahedras with a zero total magnetic moment. Remarkably, the corner-sharing geometry gives rise to a macroscopic degeneracy of the ground state.[2,3] By macroscopic, we mean that the energy of the kagomé or of the pyrochlore ground state is invariant under a rotation of a finite number of spins. Through these rotations, the system can explore all the spin configurations making up the ground energy level. The energy spectrum is, therefore, characterized by the existence of zero energy excitations, the so-called soft modes.[4] In particular, the soft modes associated with a small number of spins are extremely efficient in destroying a long-range magnetic order. A nonmagnetic ground state is predicted at $T \to 0$ K, with a spin-spin correlation function $\langle S_i S_j \rangle \sim \exp(-r_{ij}/\xi)$, where the correlation length ξ does not exceed twice the lattice parameter.[5] The huge reservoir of soft modes leads also to a low-energy shift of the excitation spectrum, so that an unusually highly dynamical state is predicted at low T.[6] This peculiar ground state is commonly called a cooperative paramagnet state or a ''spin liquid

state.''

Quite remarkably, a different description of quantum nature for $S=1/2$ geometrically frustrated AF networks yields similar results. As first elaborated by Anderson,[7] and validated through numerical calculations, the ground state can be constructed on spin singlet pairs and not on nonmagnetic triangles (or tetrahedras).[8] In particular, numerical studies point at the existence of a ''gap'' in the magnetic excitation spectrum of the kagomé $S=1/2$ network,[9] and maybe in the pyrochlore $S=1/2$ network.[10] The term gap is actually inappropriate as a continuum of singlet states is embedded between the singlet ground state and the first excited triplet state. These singlet excitations are in some respects the analog of the classical soft modes. A spin liquid ground state is again favored, with unusual thermodynamic properties such as a high entropy at low T.[11]

The discovery of the kagomé-based insulator $SrCr_{9p}Ga_{12-9p}O_{19}$ in 1988,[12] brought considerable attention onto geometric frustration. Since then, an intense mapping of the low-T physics of the kagomé and of the pyrochlore compounds has been carried out.[13,14] Original properties have been uncovered, encompassing anomalous SG states[15] and icelike ground states.[16] However, nowadays, only a few compounds are good candidates for a spin liquid ground state. Following Villain's early work,[17] the discrepancy between experience and theory is to be found in the perturbations to the ideal AF Heisenberg Hamiltonian with nearest-neighbor spin-spin interactions. The dilution of the network,[3,18] the interactions other than nearest-neighbor,[19] the dipolar interaction,[20] the anisotropy,[21] etc. are perturbations that differentiate the geometrically frustrated compounds and make them deviate from the ideal spin liquid behavior. Each deviation can potentially induce a long-range order, usually quite complex. In all experimental studies one must, therefore, discriminate between the properties related to geometric frustration and those related to these perturbations, which we may label by the general term of disorder.

However, even in the presence of these limiting parameters, spin-liquid-like compounds do exist.[22] More than in any other compound, spin-liquid-like properties are observed in $SrCr_{9p}Ga_{12-9p}O_{19}$ [SCGO(p),$0\leqslant p<1$]. The geometric frustration in SCGO arises from a kagomé bilayer of Heisenberg Cr^{3+} ions ($S=3/2$), a quasi-two-dimensional network of two kagomé layers connected by a triangular lattice linking layer (Fig. 1). The disorder in SCGO stems from the dilution of the Cr network by nonmagnetic Ga^{3+} ions. To date, all SCGO crystals reported in literature are nonstoichiometric ($p<1$).

Although an anomaly is observed at low T ($T_g\approx 2-4$ K for $0.6\leqslant p<1$) in the macroscopic susceptibility suggesting the occurrence of a SG state,[23–25] all the other experimental data available on SCGO point at the existence of a spin-liquid-like ground state. The neutron-diffraction pattern at $T<T_g$ is characterized by a broad peak, from which is extracted a spin-spin correlation length of twice the Cr-Cr distance ($\xi\approx 2d_{\text{Cr-Cr}}$).[26] A more refined neutron experiment showed that the diffraction pattern is in agreement with the existence of subgroups of spins (singlets, triangles, or tetrahedras) of zero magnetic moment.[27] Neutrons also revealed

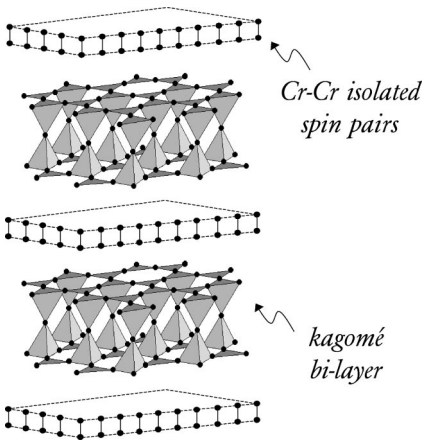

FIG. 1. The magnetic lattice of SCGO is a stacking of kagomé bilayers of Cr^{3+} ions ($\approx 78\%$ of the Cr sites), separated by Cr-Cr isolated spin pairs ($\approx 22\%$ of the Cr sites).

that only a fraction of the Cr^{3+} moment is frozen and nuon spin resonance (μSR) experiments revealed the existence of a strongly fluctuating ground state,[28,29] a picture further supported by recent specific-heat measurements, which indicate that only $\sim 50\%$ of the total entropy is removed below 100 K.[30]

From the macroscopic susceptibility (χ_{macro}), one can observe that a strong AF interaction couples the neighboring spins with a characteristic Curie-Weiss temperature $\Theta_{macro}\approx 500-600$ K. The Curie-Weiss behavior of χ_{macro} extends to temperatures $T\ll\Theta_{macro}$, which is recognized as the most typical signature of frustration.[13,14] It is puzzling that, at very low T, χ_{macro} progressively deviates from Curie-Weiss behavior and exhibits a behavior closer to a simple Curie law. This property of SCGO is actually encountered in the majority of the geometrically frustrated magnets. This is in deep contrast with the nonmagnetic ground state predicted for a spin liquid. It was conjectured that this Curie upturn might originate from the dilution, i.e., may not be an intrinsic property of the kagomé bilayer susceptibility.[31] If this is indeed the case, what is then the susceptibility of the kagomé bilayer? And what is the underlying mechanism that triggers the Curie upturn?

These are the main topics addressed in this work through the nuclear magnetic resonance (NMR) of gallium nuclei of SCGO. The ^{69}Ga and ^{71}Ga nuclei ($I=3/2$) are local probes coupled to the Cr^{3+} ions. The gallium nuclei labeled Ga($4f$) are at the heart of frustrated physics, as they are exclusively coupled to the Cr^{3+} ions of the kagomé bilayer (Fig. 2). The present NMR study was carried out on different Cr concentrations of SCGO ($0.72\leqslant p\leqslant 0.95$). The comparative study of the samples shows that Ga($4f$) NMR can discern between the geometric frustration related properties and the disorder related properties of SCGO: we are able to probe independently the kagomé bilayer susceptibility and the effects related to dilution, and thus answer both questions on a firm experimental ground.

The general outline of this paper is the following. After a detailed presentation of the samples used in this work, their characterization, and a description of their magnetic cou-

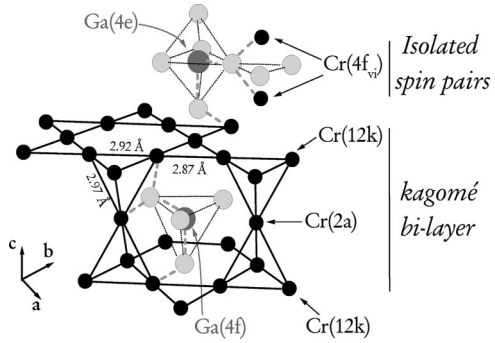

FIG. 2. The crystal structure of ideal $SrCr_9Ga_3O_{19}$. The light gray circles represent the oxygen atoms (we have restrained their number for clarity). The Sr atoms are not represented. The thick dashed lines show the typical hyperfine coupling paths of the gallium nuclei to various Cr sites through the oxygen ions.

plings (Sec. II), we focus on the specificities of the Ga NMR spectrum of SCGO: the gallium sites in SCGO, the nuclear parameters of the Ga($4f$) resonance line, and the optimization of its detection (Sec. III), with a special emphasis on the features uncovered by the study of the least diluted sample $p=0.95$. We also show that NMR is a very refined technique for characterizing the amount of Ga/Cr substitution, especially in the low dilution limit. The following sections address the main points relevant to frustrated physics. Compared to our previous study presented in Ref. 32, we provide here a deeper insight on the dilution effects. After a brief overview of the raw NMR spectra and some experimental details (Sec. IV), we present in Sec. V the first part of our comparative study. By probing the susceptibility on a local stand through the NMR shift, we identify the intrinsic, i.e., dilution-independent susceptibility, typical of the SCGO family—the archetype of geometrically frustrated compounds. We then discuss our experimental results in the light of the existing models and calculations. The main topic of Sec. VI is the study of the dilution effects. Using the NMR width, we can track down in SCGO the effect associated with the dilution of the magnetic network and isolate its contribution to the macroscopic susceptibility. Moreover, we demonstrate that the impact of the site dilution is not an effect simply localized around the substitution site. As we discuss, this sets specific constraints on the theoretical models describing the dilution effects. We finally suggest an interpretation of our NMR results based on the general context of the AF correlated systems. A summary and the concluding remarks can be found in Sec. VII.

II. SAMPLES AND MAGNETIC COUPLINGS

The Cr^{3+} ions of SCGO occupy three distinct sites, which are denoted $12k$, $2a$, and $4f_{vi}$ (Fig. 2). The Cr($12k$) sites represent 2/3 of the total number of Cr^{3+} ions and are arranged to form a kagomé lattice. The two kagomé planes are separated by a Cr($2a$) triangular layer (1/9 of the Cr^{3+} ions). The remaining 2/9 of the Cr^{3+} ions occupy the Cr($4f_{vi}$) sites. A realistic description of the Cr-Cr magnetic couplings in SCGO showed that this compound has couplings similar to Cr_2O_3.[33] As was evidenced in Ref. 33, SCGO is made up of only two magnetic entities. (1) The kagomé bilayer, i.e., the kagomé-Cr($2a$)-kagomé structure, with an average AF coupling of $J_{bilayer}\approx 80$ K as we establish in Sec. V. (2) The Cr($4f_{vi}$)-Cr($4f_{vi}$) spin pairs with an AF coupling of $J_{pair}=216(2)$ K, each pair being isolated from the others. The full structure is obtained by the stacking: spin pairs/kagomé bilayer/spin pairs/kagomé bilayer, etc. The interaction between the kagomé bilayer and the spin pairs is small (~ 1 K). Since all the Cr($4f_{vi}$) spin pairs form nonmagnetic singlets at low T ($T \ll J_{pair}$, see the Appendix), the low-T properties of SCGO are expected to reflect those of the kagomé bilayer network only.

TABLE I. The characteristic susceptibility parameters for some of the SCGO samples studied. μ_{eff} and Θ_{macro} are extracted by fitting the high-T behavior of χ^{-1}_{macro} ($T \geqslant 150$ K) to a Curie-Weiss law.

p	μ_{eff}	Θ_{macro} (K)	T_g (K)
0.72	$3.85(5)\mu_B$	356(11)	2.3
0.81	$4.00(2)\mu_B$	439(7)	3.3
0.89	$4.05(2)\mu_B$	501(7)	3.5
0.90	$4.21(1)\mu_B$	560(5)	3.2
0.95	$4.23(2)\mu_B$	608(7)	3.6

From the previous considerations, it is quite clear that the kagomé bilayer structure is more complex to model than a pure kagomé system. However, SCGO is ideal in many regards. As mentioned in the Introduction, the interactions in the magnetic Hamiltonian other than a nearest-neighbor interaction, are likely to modify the spin liquid nature of the ground state. These interactions are here extremely small compared to the Cr-Cr interaction in the kagomé bilayer. The anisotropy of Cr^{3+} is ≈ 0.08 K (spins are, therefore, of Heisenberg nature),[34] the dipolar interaction is ~ 0.1 K, and the next-nearest-neighbor interactions J_{nnn} are most likely $|J_{\mathrm{nnn}}|<4$ K, as in Cr_2O_3.[35] These microscopical details might not be totally uncorrelated with the spin-liquid-like behavior observed in SCGO.

The present study was performed on a series of seven values of Cr content, corresponding to concentrations of $p=0.72,0.81,0.89,0.90,0.91,0.93,0.95$. All the samples are ceramics and were synthesized by a solid-state reaction of $SrCO_3$, Cr_2O_3, and Ga_2O_3 in air at 1350 °C, typical for SCGO. The reaction products were checked by x-ray diffraction and by macroscopic susceptibility measurements. The physical parameters for χ_{macro} yielded results in agreement with literature (Table I). More refined characterizations were also performed. The $p=0.81,0.89,0.95$ samples were investigated by high-resolution neutron diffraction with the D2B spectrometer of the Institut Laue-Langevin in order to estimate the occupation of the three Cr sites of SCGO, respectively, p_{12k}, p_{2a}, and $p_{4f_{vi}}$, otherwise nonmeasurable by x-ray diffraction. The results are presented in Fig. 3. The $p=0.72$ and 0.90 samples were the object of μSR studies.[28,29] Finally, the Cr concentration of the samples was also checked directly by Ga NMR (detailed in Sec. III).

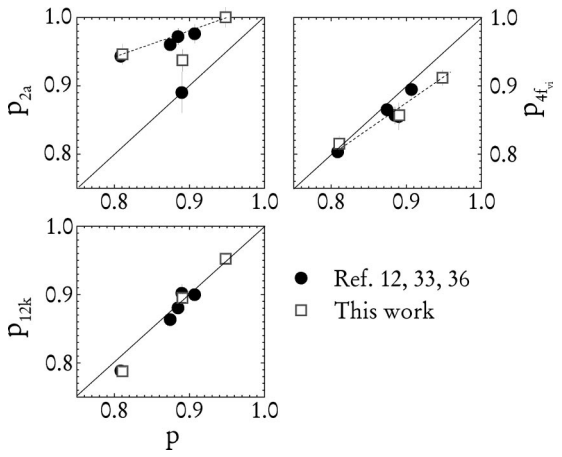

FIG. 3. The relative Cr concentration on the $12k$, $2a$, and $4f_{vi}$ sites determined by the neutron measurements (p_{12k},p_{2a},$p_{4f_{vi}}$) versus the overall Cr concentration (p) of our $p=0.81,0.89,0.95$ samples (open squares) and of other samples in the literature (closed circles). The Cr concentration of the three sites follows stoichiometry when the symbols fall on the solid line.

The synthesis of samples with higher Cr content than $p=0.95$ failed. The x-ray diffraction showed a Cr_2O_3 parasitical presence of $\gtrsim 0.5\%$ (our detection threshold) in the final product of $p=0.95$ and all the additional Cr_2O_3 introduced in the solid-state reaction to reach higher concentrations than $p=0.95$ simply did not react. This sets the limit of this synthesis method to the $p=0.95$ concentration. Interestingly, this limit may be related to the fact that the Ga/Cr substitution in SCGO is not uniform, i.e., the Cr concentration is not equal to p on all the sites. As shown in Fig. 3, the Ga/Cr substitution on the Cr($12k$) sites corresponds to stoichiometry ($p \approx p_{12k}$), whereas in contrast the Cr($2a$) sites are robust to substitution ($p_{2a} > p$), the nonstoichiometric gallium occupying preferentially the Cr($4f_{vi}$) sites ($p_{4f_{vi}} < p$).[12,33,36] We note that no gallium is present on the Cr($2a$) sites of the $p=0.95$ sample and that concomitantly the parasitical Cr_2O_3 problem occurs at this same Cr concentration, an indication that the two phenomena may be related to the same chemical constraint.

A last point we would like to address is the influence of the Ga/Cr substitution on the crystal parameters a and c. The largest structural change we observed is an elongation of ≈ 0.004 Å of the Cr($12k$)-Cr($2a$) distance in the $p=0.72$ sample (2.975 Å) compared to the $p=0.95$ sample (2.971 Å). A study on a series of chromium-based oxides with Cr-O-Cr bonding angles $\sim 90°$ (as in SCGO) showed that the Cr-Cr exchange constant decreases linearly with increasing Cr-Cr distance (Fig. 4) with a slope of $\Delta J/\Delta d_{\text{Cr-Cr}} \approx 450$ K/Å,[37] from which we extract a negligible variation of the SCGO exchange constants at most of $\Delta J \approx 3$ K. We, therefore, expect the sizeable *variation of the magnetic properties of SCGO with p* to reflect only the effect of the lattice *dilution.*

III. Ga NMR SPECTRUM

The present NMR study was performed on the ^{69}Ga ($^{69}\gamma = 10.219$ MHz/T, $^{69}Q = 0.178 \times 10^{-24}$ cm^2) and the

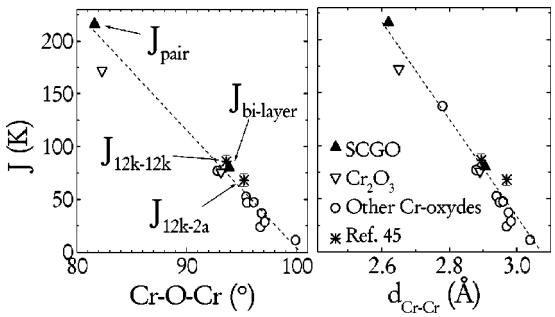

FIG. 4. The Cr-Cr couplings as a function of the Cr-O-Cr angle (left) and the Cr-Cr distance (right) for the average Cr-Cr coupling of the SCGO kagomé bilayer (see Sec. V B), the SCGO Cr($4f_{vi}$)-Cr($4f_{vi}$) pairs (Ref. 33), Cr_2O_3 (Ref. 35), and a series of Cr oxides (Ref. 37). The stars stand for the Cr($12k$)-Cr($12k$) and the Cr($12k$)-Cr($2a$) couplings of SCGO's kagomé bilayer, which we determined in a previous paper via a refined analysis of the NMR shift (Ref. 45).

^{71}Ga ($^{71}\gamma = 12.982$ MHz/T, $^{71}Q = 0.112 \times 10^{-24}$ cm^2) nuclei of SCGO powder samples (γ and Q are, respectively, the gyromagnetic ratio and the quadrupolar moment of the nucleus). The gallium ions are present on two distinct crystallographic sites, which are designated by Ga($4f$) and Ga($4e$) (Fig. 2). A previous spectral analysis, carried out on the $p=0.90$ sample in a sweep field set up at a radio frequency of $\nu_{rf} = 131$ MHz, successfully assigned each site to the corresponding peak in the NMR spectrum.[38] There, it was shown that the Ga NMR spectrum of both isotopes is actually the sum of three contributions: Ga($4f$), Ga($4e$), and an extra contribution related to the presence of nonstoichiometric gallium on the Cr sites, which we label by Ga(sub).

As was pointed out in Ref. 38, the interest of Ga NMR resides in the fact that the gallium nuclei are coupled to the neighboring magnetic Cr^{3+} ions through a Ga-O-Cr hyperfine bridge (Fig. 2). In particular, the ^{69,71}Ga($4f$) nuclei are exclusively coupled to the kagomé bilayer, nine from the two kagomé adjacent Cr($12k$) layers and three from the intermediate Cr($2a$) sites. Through Ga($4f$) NMR we are then able to probe locally the magnetic properties of the kagomé bilayer. The present NMR study is, therefore devoted to Ga($4f$) NMR.

Along with the hyperfine interaction mentioned here above, the nuclear Hamiltonian of gallium in SCGO also bears an additional quadrupole interaction due to the electric field gradient (EFG) on the gallium sites. Following the usual notations, the nuclear Hamiltonian may be expressed as

$$\mathcal{H} = -h\gamma \vec{I} \cdot (\overleftrightarrow{1} + \overleftrightarrow{K}) \cdot \vec{H} + \frac{h\nu_Q}{6}[3I_z^2 - I^2 + \eta(I_x^2 - I_y^2)],$$

where $\vec{H}$ is the applied field, the principal axes of the magnetic shift tensor $\overleftrightarrow{K}$ are collinear with the direction of the nuclear-spin operators I_x, I_y, and I_z, ν_Q is the quadrupole frequency, and $0 \leqslant \eta \leqslant 1$ is the quadrupole asymmetry parameter. The main focus of the spectral analysis presented in

TABLE II. The quadrupole parameters of the $4e$ and $4f$ gallium nuclei in SCGO. The ^{69}Ga isotope yields a stronger quadrupole interaction compared to the ^{71}Ga isotope, since the quadrupole moments are in a ratio of $^{69}Q/^{71}Q = {}^{69}\nu_Q/{}^{71}\nu_Q = 1.589$.

	$^{71}\nu_Q$ (MHz)	$^{69}\nu_Q$ (MHz)	η
Ga($4e$)[a]	20.5(3)	32.6(5)	0.050(35)
Ga($4f$)[b]	2.9(2)	4.6(2)	0.005(6)

[a]From Ref. 38.
[b]This work.

this section is to complete the study of Ref. 38 by determining the quadrupole contribution to the nuclear Hamiltonian of Ga($4f$), working in a frequency range ($\nu_{rf} = 40.454$ MHz) more appropriate for the observation of the ^{69,71}Ga($4f$) resonance lines. We study here the spectrum of the $p = 0.95$ sample, which yields sharper quadrupole features than the $p = 0.90$ sample (or of any of the other samples studied). The knowledge of the quadrupole parameters reported in Table II allows us, in the following section, to separate the magnetic and the quadrupole contributions to the Ga($4f$) spectrum and, hence, to safely evaluate the magnetic properties of the kagomé bilayer.

In the second part of this section we focus on Ga(sub). We identify the contribution of Ga(sub) to the spectrum acquired at $\nu_{rf} = 40.454$ MHz and, on the basis of this contribution, provide a method to evaluate the Cr concentration of the SCGO samples through Ga NMR, especially well suited for the very low dilutions.

A. Spectral analysis of Ga($4f$)

Neglecting the Ga-substituted sites, the Ga NMR spectrum displays four sets of lines corresponding to the two isotopes distributed on both Ga($4e$) and Ga($4f$) sites. In a powder, for a given site and a given isotope, the line-shape results from the distribution of the angles between the field and the EFG principal axis. This yields singularities rather than well defined peaks—the so-called powder line shape.

The quadrupole interaction of gallium nuclei in SCGO is a consequence of the coupling of the nucleus to the EFG produced by the surrounding electronic charges, here mainly the oxygen ions. As shown in Fig. 2, Ga($4e$) is surrounded by a bipyramid of five oxygen ions. This environment has no local cubic symmetry and results in a strong quadrupole frequency as was evidenced in Ref. 38 (Table II). In contrast with Ga($4e$), Ga($4f$) is surrounded by a nearly ideal tetrahedron of oxygens ions, only slightly elongated along the crystalline $\vec{c}$ axis. Since a regular tetrahedron has a local cubic symmetry, we expect the quadrupole frequency of Ga($4f$) to be $\nu_Q(4f) \ll \nu_Q(4e)$. This agrees with Ref. 38 where the Ga($4f$) quadrupolar effects were not detected at a frequency of $\nu_{rf} = 131$ MHz. The asymmetry parameter η, which quantifies the deviation of the EFG from axial symmetry, is, in principle, close to zero for both sites as they share a rotation axis along $\vec{c}$.

We present in the top panel of Fig. 5 a field sweep spectrum, obtained at $\nu_{rf} = 40.454$ MHz and $T = 80$ K for the

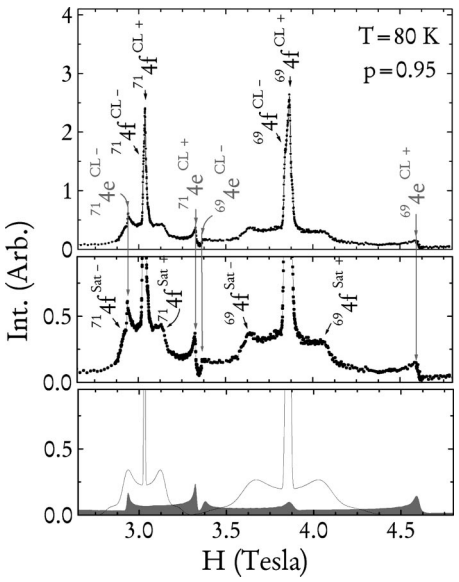

FIG. 5. Top panel: A field sweep of ^{71}Ga and ^{69}Ga at $\nu_{rf} = 40.454$ MHz. The site and transition assignments of each peak are described in the text. Middle panel: The satellite transitions in the ^{69,71}Ga($4f$) line. The satellite singularities of the $4e$ line are not resolved. Bottom panel: A line simulation of ^{69,71}Ga($4f$) (solid line) and of ^{69,71}Ga($4e$) (dark gray area) performed on the basis of the quadrupole parameters of Table II. The simulated spectrum does not account for the Ga(sub) contribution.

$p = 0.95$ sample. The sweep, from 2.65 T to 4.80 T, covers the spectrum of both isotopes and yields the expected features. We first focus on the ^{69,71}Ga($4e$) line. A powder sample simulation of the $4e$ line is presented in the bottom panel of Fig. 5 to emphasize its contribution to the spectrum. Each $4e$ isotope, i.e., ^{71}Ga($4e$) and ^{69}Ga($4e$), exhibits a resonance in a wide range of fields, with multiple quadrupole peaks and steps associated with the three nuclear Zeeman transitions $3/2 \leftrightarrow 1/2$, $1/2 \leftrightarrow -1/2$, and $-1/2 \leftrightarrow -3/2$. As evidenced in Fig. 5, in this field window only the $1/2 \leftrightarrow -1/2$ resonance transition is resolved yielding for each $4e$ isotope two singularities known as the central line singularities (labeled, respectively, by CL− and CL+ in Fig. 5). These two singularities are the boundaries of the central line splitting of width $\approx \nu_Q^2/2\gamma\nu_{rf}$.[39] Compared to the working frequency of $\nu_{rf} = 131$ MHz used in Ref. 38, the much lower frequency of $\nu_{rf} = 40.454$ MHz allows here to spread the $4e$ line over a wider field range. The ^{69,71}Ga($4e$) contribution to the spectrum is a nearly constant background of small amplitude compared to the ^{69}Ga($4f$) and ^{71}Ga($4f$) lines—the two prominent peaks of Fig. 5—hence there is a better contrast between the sites. Furthermore, overlap between the Ga($4e$) and Ga($4f$) lines is also minimized at this radio frequency.

We now focus on the ^{69,71}Ga($4f$) line of Fig. 5. In these favorable experimental conditions, it can be seen that both $4f$ peaks are flanked by two shoulders, the so-called satellite singularities (labeled, respectively, by Sat− and Sat+ in the middle panel of Fig. 5), associated with the $3/2 \leftrightarrow 1/2$ (Sat−) and the $-1/2 \leftrightarrow -3/2$ (Sat+) nuclear transitions. The detection of the satellite singularities is a clear indication of the existence of quadrupole effects in the ^{69,71}Ga($4f$)

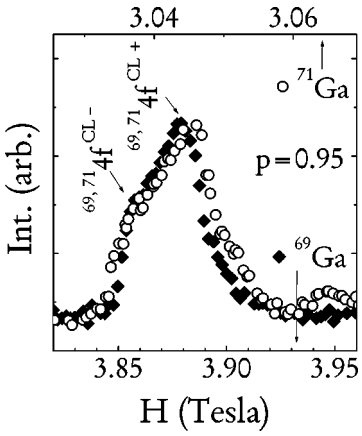

FIG. 6. Field sweeps of the ^{69}Ga($4f$) and the ^{71}Ga($4f$) lines at $T=150$ K. The closed (open) symbols represent ^{69}Ga (^{71}Ga). The top abscissa is scaled to the bottom by a factor $^{69}(Q^2/\gamma)/^{71}(Q^2/\gamma)=3.209$ to evidence the quadrupole structure in the lines. The hump at ≈ 3.065 T is ^{71}Ga(sub).

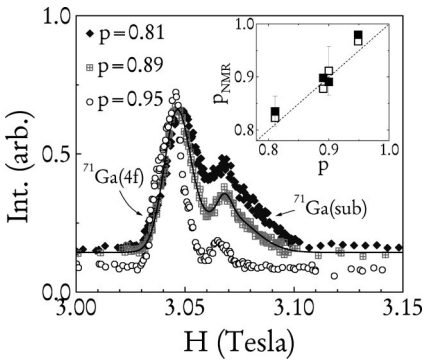

FIG. 7. A field sweep centered on the ^{71}Ga($4f$) central line performed at $T=150$ K. The solid line is a multiple Gaussian fit. Inset: p_{NMR} versus p. The open and closed symbols are, respectively, the Cr concentration evaluated by direct integration and by multiple Gaussian fits. The dashed line is the expected value from neutron/x-ray diffraction.

spectrum, implying also a central line splitting for Ga($4f$). To emphasize this central line splitting, we present in Fig. 6 narrow field sweeps of both isotopes at $T=150$ K. The sweep ranging from 3.820 T to 3.960 T covers the ^{69}Ga($4f$) line (bottom abscissa) whereas the sweep ranging from 3.026 T to 3.069 T covers the ^{71}Ga($4f$) line (top abscissa). As shown, the two central lines match since we expanded the field window of ^{71}Ga($4f$) by a factor $^{69}(Q^2/\gamma)/^{71}(Q^2/\gamma)=3.209$, i.e., by the ratio of the central line quadrupolar widths expected for the two isotopes. Figure 6 also indicates that the structure observed in the $4f$ line is dominated, at these temperatures, by quadrupole effects. In particular, the anisotropy in the shift $\vec{\vec{K}}$, which could, in principle, yield additional structure to the line, is small, i.e., the shift is isotropic ($\vec{\vec{K}} \equiv K$). This conclusion is further supported by a calculation, presented below, of *all* the field singularities.

We now turn to the evaluation of the quadrupole parameters of ^{69,71}Ga($4f$). This was carried out using the field positions H_{sing} of the quadrupole singularities determined from Fig. 5 and reported in Table III, which depend only on the three parameters $\nu_Q(4f)$, $\eta(4f)$, and K, provided the shift is isotropic: $H_{sing}=H(\nu_Q,\eta,K)$.[39] We evaluated the $4f$ quadrupole parameters from the singularity positions of ^{69}Ga$(4f)^{Sat-}$, ^{69}Ga$(4f)^{CL+}$, and ^{69}Ga$(4f)^{Sat+}$. At $T=80$ K, the shift is $K=0.0285(5)$. The extracted quadrupole parameters are presented in Table II and are found in agreement with expectations. To confirm the isotropic nature of the shift, we performed a self-consistency test by calculating the field positions of all the quadrupole singularities in Fig. 5. This is readily done using the three parameters $\nu_Q(4f)$, $\eta(4f)$, and K determined previously and the set of equations of Ref. 39. As shown in Table III, the calculated positions are in excellent agreement with the experimental ones.

Finally, concerning the quadrupole interaction in all the other SCGO samples studied, no appreciable change was evidenced in $\nu_Q(4f)$ and $\eta(4f)$. In conclusion, the Ga($4f$) central line is narrow enough in all the samples to allow following accurately the T variation of the shift and of the linewidth.

B. Gallium substituted on the Cr sites

In Fig. 7 we compare the ^{71}Ga spectra obtained for the $p=0.81$, 0.89, 0.95 samples at $T=150$ K and $\nu_{rf}=40.454$ MHz. Care was taken to ensure the same experimental conditions. The field sweeps of Fig. 7 cover a narrow field window δH (from 3.00 T to 3.15 T) centered on the central line of ^{71}Ga($4f$) ($H\approx 3.05$ T). Two features differ between the samples: (1) The line at $H\approx 3.065$ T, whose integrated area decreases with increasing p, which is, therefore, ^{71}Ga(sub); (2) the constant background $b(p)$, which decreases with increasing p. ^{71}Ga(sub) and a part of $b(p)$ are, therefore, all the contributions of the nonstoichiometric gallium to the ^{71}Ga spectrum.[40]

TABLE III. The field positions of the $4f$ quadrupole singularities in Fig. 5. H_{sing} are the fields where each singularity was found experimentally and H_{sing}^{calc} are the calculated fields where the singularities are expected. The missing H_{sing}^{calc} correspond to the field singularities used to perform the calculation.

Sing.	$^{71}H_{sing}$ (T)	$^{69}H_{sing}$ (T)	$^{71}H_{sing}^{calc}$ (T)	$^{69}H_{sing}^{calc}$ (T)
$4f^{CL-}$	3.025(2)	3.838(1)	3.026(2)	3.838(2)
$4f^{CL+}$	3.036(1)	3.865(1)	3.035(2)	
$4f^{Sat-}$	2.924(9)	3.628(8)	2.921(9)	
$4f^{Sat+}$	3.137(7)	4.066(8)	3.138(7)	

Since the nonstoichiometric gallium is present on the three Cr sites of SCGO, one would expect to detect three gallium lines and not a unique Ga(sub) line. To gain insight into this problem, we studied the spectrum of the parent and nonmagnetic compound $SrGa_{12}O_{19}$ ($p=0$). The spectrum allows to evidence sizeable quadrupole effects on the $12k$ [$^{71}\nu_Q=5.1(1)$ MHz and $\eta=0.47(3)$] and on the $4f_{vi}$ [$^{71}\nu_Q=1.6(1)$ MHz and $\eta=0.03(5)$] substituted sites, otherwise nonmeasurable in the magnetic compounds ($p\neq 0$).[41] The quadrupole effects on the $2a$ site are negligible ($^{71}\nu_Q \approx 0.3$ MHz and $\eta\approx 0$). Turning back to the spectra of Fig. 7, the ^{71}Ga(sub) line is the unresolved sum of the $2a$ line and of the $12k$ and $4f_{vi}$ quadrupole central lines of substituted gallium, whereas the background $b(p)$, in addition to the Ga($4e$) and Ga($4f$) satellite contributions mentioned in Sec. III A, contains the sum of the satellite contributions of the substituted gallium.

In order to evaluate the Cr concentration of our samples using Ga NMR (p_{NMR}), we determine the intensities I_{4f} and $I_{sub}(p)$ of, respectively, the ^{71}Ga($4f$) central line and the ^{71}Ga(sub) line of Fig. 7. To do so, we evaluate the integrated area of both lines corrected for the transverse exponential relaxation [T_2(sub)$=78(2)$ μs and $T_2(4f)=50(1)$ μs]. $I_{sub}(p)$ and I_{4f} are, respectively, proportional to the amount of gallium present on the three substitution sites and on the $4f$ site. The lines are well separated in the $p=0.95$ sample, so that $I_{sub}(p)$ and I_{4f} are evaluated separately. For the more diluted samples, the intensity I_{4f} is fixed to the $p=0.95$ value as the amount of gallium on the $4f$ site is independent of Cr concentration. $I_{sub}(p)$ was then evaluated either by direct integration of the spectrum over the field window δH and subsequent subtraction of both $b(p)\delta H$ and I_{4f}, or by reproducing all the lines with a minimal three-Gaussian fit and an additional constant background $b(p)$ [one Gaussian for the ^{71}Ga($4f$) line with an intensity fixed to the $p=0.95$ value, and two Gaussians for ^{71}Ga(sub), the area of which yields I_{sub}]. From the ratio I_{sub}/I_{4f}, we can extract p_{NMR}. In the inset of Fig. 7 we show the variation of p_{NMR} with the concentration p determined by x-ray and neutron diffraction. Whatever the method employed (integration or multiple Gaussian fits), we notice a perfect agreement between the different characterization methods. Since p_{NMR} is equal to p, we conclude that the actual chemical content corresponds to the nominal concentration.

Incidentally, Ga NMR proves to be quite an accurate tool for determining the Cr concentration in SCGO, especially for dilutions as low as 5% or less where the other techniques are beyond their sensitivity limit. For the samples with $p>0.95$, we did not find any further decrease of the I_{sub} value, which confirms *locally* that it is impossible to synthesize samples beyond the $p=0.95$ limit found through x-ray diffraction.

IV. DILUTION AND *T* DEPENDENCE OF THE Ga(4*f*) SPECTRUM

To appreciate the experimental evidence of the properties we discuss in the following sections, we present here the dilution and the T dependence of the raw ^{71}Ga($4f$) NMR spectra. The main relevant physical parameters of interest are the shift of the line, which as we establish allows us to probe directly the susceptibility of the kagomé bilayer, and the linewidth, which in contrast yields information on the distribution of the internal local fields in the kagomé bilayer. We also briefly describe the analysis performed to extract these spectral parameters.

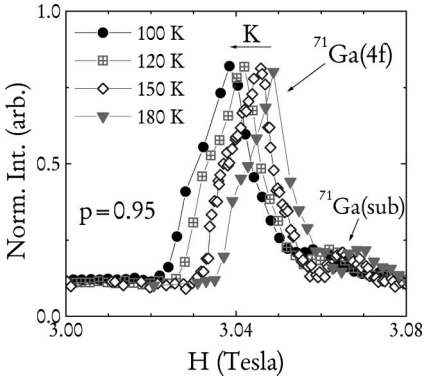

FIG. 8. Typical high-T field sweeps of the ^{71}Ga($4f$) central line.

A. Experimental data

The Ga($4f$) spectra were recorded in a wide T range, from 5 K to 410 K. Up to 200 K, the spectra were obtained in a sweep field set up with a working frequency of $\nu_{rf}=40.454$ MHz. For 150 K$\leqslant T\leqslant$410 K, the spectra were recorded in a static field of $\approx$7 T by a swept-frequency variant of the field step spectroscopy method.[42] Our data can be sorted in two distinct temperature domains, typically $T\geqslant 100$ K and $T<100$ K.

A typical series of high-T spectra (100 K$\leqslant T\leqslant$180 K) is presented in Fig. 8 for the $p=0.95$ sample. The field window (from 3.00 T to 3.08 T) covers the central line of ^{71}Ga($4f$). Figure 8 is representative of the evolution of Ga($4f$) at $T\geqslant 100$ K for all the samples studied. The line shape is nearly constant with temperature, as dominated by T-independent quadrupole effects, and shifts towards low fields with decreasing temperature. The shift K, which is experimentally measured by the position of the ^{71}Ga$(4f)^{CL+}$ singularity and by performing minor quadrupole corrections (see Sec. III), therefore increases when the temperature is lowered.

The T dependence of both K and the width changes at low T. We present in Fig. 9 spectra ranging from 5 K to 50 K for the $p=0.95$ sample (top) and the $p=0.81$ sample (bottom). The field window covers the ^{71}Ga($4f$) line, but is larger than in Fig. 8, from 2.90 T to 3.15 T. Three important features should be noticed.

(1) The line now shifts toward the high fields and hence K is decreasing with the temperature. However K does not reach the zero value, i.e., the ^{71}Ga($4f$) line is never centered at the reference value $^{71}H_{ref}=\nu_{rf}/^{71}\gamma=3.116$ T. The comparison of the two series of spectra establishes that the change in the shift direction is not affected by the dilution.

(2) The width increases with decreasing temperature. The quadrupole structure that can still be noticed on the $T=50$ K spectrum of the $p=0.95$ sample is progressively

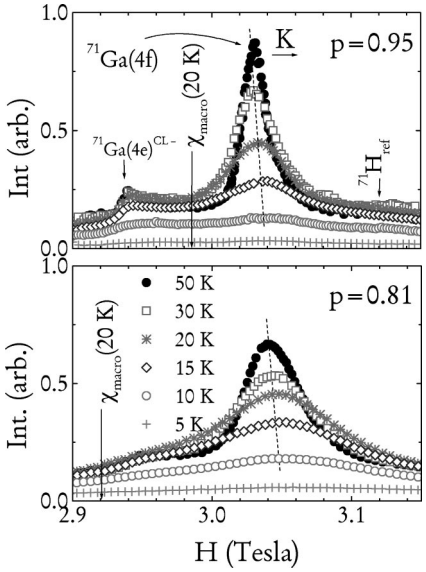

FIG. 9. Low-T field sweeps of ^{71}Ga$(4f)$ for the $p=0.95$ sample (top panel) and the $p=0.81$ sample (bottom panel). The dashed line is a guide to the eye.

washed away as temperature is lowered. At $T=20$ K, the line is marked by a smooth symmetric broadening of a Gaussian nature. This broadening is more important for the $p=0.81$ sample than for the $p=0.95$ sample, i.e., the width is sensitive to the dilution. The ^{71}Ga(sub) line is no longer resolved in this T domain.

(3) A last feature we would like to underline is the abrupt decrease of the detected ^{69,71}Ga$(4f)$ nuclear population at $T<15$ K in both samples. The nuclear population, proportional to the integrated area of the $4f$ line, actually decreases in the same way in all the samples studied (Fig. 10). It, therefore, originates from a dilution-independent mechanism. The present result confirms the conclusions of the previous Ga$(4f)$ NMR study on the $p=0.90$ sample.[32] There, the wipeout of the intensity was assigned to originate from the

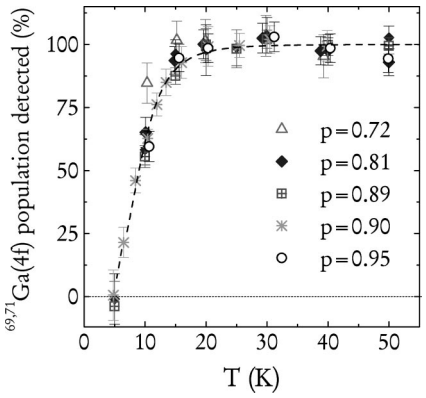

FIG. 10. The ^{69,71}Ga$(4f)$ population detected by NMR. For each sample, the integrated area of the $4f$ line is normalized by the integrated area measured in the 20–50 K temperature range, where it is found constant in temperature. The Ga$(4e)$ contribution, constant in temperature, was subtracted. T_2 corrections were found quite small and do not affect estimates below 50 K.

intrinsic high dynamics of the kagomé bilayer spin system when $T\rightarrow 0$ K. This effect, explicitly evidenced in SCGO by μSR measurements,[28,29] is taken to be the signature of a spin-liquid-like ground state. Because of this abrupt decrease of the NMR signal, ^{69,71}Ga$(4f)$ is not a suitable probe for $T<10$–15 K. The comparison of the spectra of all the samples enables us in the following sections to easily separate the properties related to the dilution from the intrinsic properties independent on the dilution.

B. NMR line analysis

Compared to Ref. 32, we employed here a different method to evaluate the shift K and the width ΔH of the spectra of Fig. 9. (i) For all the samples, we choose a ^{69,71}Ga$(4f)$ high-T reference spectrum dominated by T-independent quadrupole effects $[\mathcal{S}_Q(H)]$. (ii) In order to recover the low-T broadening of Gaussian nature, $\mathcal{S}_Q(H)$ is convoluted by a normalized Gaussian function $G(H)$ of width ΔH. Since it is impossible to fit separately the substituted and nonsubstituted sites, we explicitly assume that for the highly diluted samples both sites broaden identically. This is likely the case in view of the hyperfine coupling paths. The low T spectrum $\mathcal{S}_M(H)$ is, therefore, simply reproduced by

$$\mathcal{S}_M(H)=a\left[y_0+\int_{-\infty}^{+\infty}G(H-H')\mathcal{S}_Q(H'+H_s)dH'\right],$$

where H_s is the field shift of $\mathcal{S}_Q(H)$ from which we extract K. Since the ^{69,71}Ga$(4f)$ line lies on a constant background that results mainly from the contribution of the second gallium site Ga$(4e)$ (see Fig. 5), the amplitude a and the constant background y_0 are employed to readjust the relative spectral weights of the $4e$ and of the $4f$ lines when the transverse relaxation T_2 corrections vary differently on the two gallium sites.[43] We also restricted our fits to the left side of the line, very sharp at high T and which has the major advantage of not being affected by the Ga/Cr substitutions. Concerning the values of K, we did not find any significant difference with the method employed in Ref. 32.

C. Magnetic contribution to the Ga$(4f)$-NMR line: Shift and width

We briefly recall here the relationship between the contribution of each gallium nucleus to the Ga$(4f)$ NMR line and its local magnetic environment in order to underline what can be exactly probed through Ga$(4f)$ NMR (more details can be found in Refs. 38, 41, and 45).

Each Ga$(4f)$ nucleus is coupled to its Cr$(12k)$ and Cr$(2a)$ nearest neighbors (nn) through a Ga-O-Cr hyperfine interaction with a hyperfine constant $\mathcal{A}$.[44] We suppose that the susceptibility in the kagomé bilayer varies from Cr site to Cr site and label it, in a generic manner, by χ. A Ga$(4f)$ at site i will contribute to the NMR spectrum at a position depending upon the number of the nn occupied Cr sites and their susceptibility χ. This corresponds to the shift $K^{(i)}$ in the NMR spectrum for gallium at site i,

$$K^{(i)} = \sum_{\text{occupied nn Cr}(12k,2a)} \mathcal{A}\chi$$

(the chemical shift is negligible). The average shift of the NMR line, which we label by K in the following sections, is simply related to the average susceptibility $\overline{\chi}$ over all the Cr sites. As we establish, the shift corresponds to the frustrated susceptibility χ_{frustr}, so that $K \propto \chi_{frustr}$. Instead, the spatial distribution of $K^{(i)}$ around K defines the magnetic width of the Ga NMR spectrum and reflects the existence of a spatial distribution of χ (as we detail in Sec. VI B, a spatial distribution of the hyperfine constant or a distribution related to the presence of Cr vacancies in the nuclear environment is negligible and cannot justify the low-T broadening observed).

V. KAGOMÉ BILAYER SUSCEPTIBILITY: EVIDENCE FOR CORRELATIONS EFFECTS

As mentioned in the preceding section, the shift K measures the average kagomé bilayer susceptibility that proves to be unobservable at low T through the macroscopic susceptibility measurements. We show here that the T dependence of K gives a sharp evidence for a maximum in the susceptibility χ_{frustr} around 50 K, whatever the amount of dilution. The comparison of our results on the SCGO compound with the different models existing in the literature does not allow us to totally validate or invalidate them. Our observations rather favor an image, supported by recent neutron-diffraction data, where the short-range magnetic correlations play a central role.

A. An intermediate temperature scale

The T dependence of K for the $p=0.81,0.89,0.95$ samples is presented in Fig. 11. The figure is the quantitative evaluation of the line shifts of Figs. 8 and 9. K increases following a Curie-Weiss law (see below) up to a temperature of $T_{max}=40-50$ K, where it reaches a maximum. Below T_{max}, K decreases, but does not reach zero for the observed temperatures ($T \geqslant 15$ K). The decrease in K is slightly more pronounced with increasing dilution. For the $p=0.81$ sample, $K(T=15\ \text{K})/K(T_{max}) \approx 0.86$, instead of 0.92 for the $p=0.95$ sample. Although for $T<15$ K the measurement of K is less significant since a wipeout of the intensity occurs, we observed in the $p=0.90$ sample only a decrease of $K(T=7\ \text{K})/K(T_{max}) \approx 0.77$.[32]

The typical T variation of K^{-1} is presented in the inset of Fig. 11 for the $p=0.95$ sample. The high-T variation of K^{-1} ($T \geqslant 100$ K) is linear for all the samples, suggesting a Curie-Weiss behavior. A linear extrapolation to $K^{-1}=0$ yields the Curie-Weiss temperature as determined by NMR (Θ_{NMR}). The values of Θ_{NMR} are 453(30) K, 469(27) K, and 484(25) K for the $p=0.81,0.89,0.95$ samples, respectively. We find here in K a well-known property of the susceptibility of the geometrically frustrated compounds: the Curie-Weiss behavior continues to subsist at temperatures $T \ll \Theta_{NMR}$.

Assuming the Curie-Weiss value of the kagomé bilayer to be $\langle z \rangle J_{bilayer} S(S+1)/3k_B$, where $\langle z \rangle = 5.14$ is the average number of nearest neighbors for a Cr site of the kagomé bilayer as the Cr environments of the Cr($2a$) and the Cr($12k$) sites differ, we find an average exchange constant of $J_{bilayer} \approx 80$ K. As shown in Fig. 4, this value is close to the exchange constant $J=76(3)$ K observed in Cr_2O_3 where the Cr^{3+} ions have a local octahedral environment similar to Cr($12k$).[35] We also gained more insight on the couplings of the kagomé bilayer through a mean-field analysis of the high-T shift, detailed in Ref. 45, which allowed us to evaluate the Cr($12k$)-Cr($2a$) and the Cr($12k$)-Cr($12k$) couplings (their values are reported on Fig. 4). Turning back to the NMR Curie-Weiss temperature, Θ_{NMR} is of the same order as the macroscopic Curie-Weiss temperature, although smaller with an increasing difference at higher Cr concentrations. This difference is related to the fact that the susceptibility of the Cr($4f_{vi}$)-Cr($4f_{vi}$) isolated spin pairs also contributes to χ_{macro}, but is absent in K since the Ga($4f$) nuclei probe only the susceptibility of the kagomé bilayer (Sec. V B).

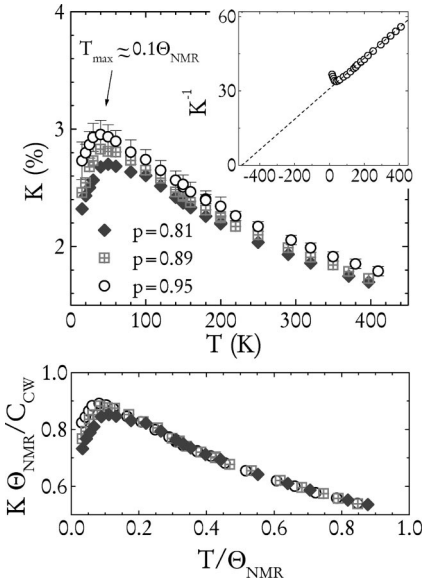

FIG. 11. Top panel: K versus T down to 15 K. A minor second-order quadrupole correction has been performed. Inset: K^{-1} versus T for $p=0.95$. Bottom panel: K versus T plotted using reduced units. C_{CW} and Θ_{NMR} are, respectively, the Curie-Weiss constant and temperature extracted from the high-T Curie-Weiss fit to K^{-1} described in the text.

The linear behavior of K for $T \ll \Theta_{NMR}$ and the deviation from this behavior that results in a maximum in K versus temperature is a common feature of the three samples. It then stems from a physics robust on dilution, therefore related to an intrinsic property of the kagomé bilayer. T_{max} is a new temperature scale for SCGO since it differs substantially from the two known characteristic temperatures, the freezing temperature T_g ($T_{max}/T_g \approx 10$) and the Curie-Weiss temperature ($T_{max}/\Theta_{NMR} \approx 0.1$).

B. Evidence for a two-component macroscopic susceptibility

We compare in Fig. 12 the T dependence of K (left y axis) and of χ_{macro} (right y axis) for the $p=0.95$ sample. The

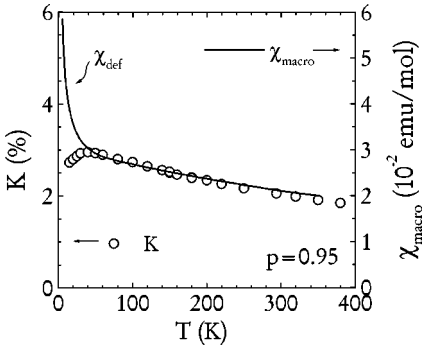

FIG. 12. K (left) and χ_{macro} (right) for the $p=0.95$ sample. K and χ_{macro} do not follow exactly the same law at high T, since χ_{macro} probes also the susceptibility of the Cr($4f_{vi}$)-Cr($4f_{vi}$) spin pairs.

discrepancy between the low-T behavior of K and χ_{macro} is quite clear since instead of a maximum in the susceptibility, χ_{macro} exhibits a Curie-like law at low T. The difference between K and χ_{macro} is also perceptible directly on the spectra of Fig. 9 where an arrow indicates the approximate position where the maximum of the ^{71}Ga($4f$) line should occur if $K \propto \chi_{macro}$. Instead of a model where χ_{macro} has a single component, our results establish that χ_{macro} yields at least two distinct contributions. The first one is χ_{frustr}, spatially uniform over the kagomé bilayer and which is reflected in K (Sec. IV C). A second one, nonuniform over the Cr sites, which is necessary to explain the Curie-like upturn observed at low T. We label this contribution as χ_{def}, since in Sec. VI we establish that χ_{def} is the susceptibility of the magnetic defects generated by the dilution of the kagomé bilayer. The comparison of Fig. 12 establishes on an experimental ground the conjecture by Schiffer and Daruka of a two-component macroscopic susceptibility.[31]

The macroscopic susceptibility probes both contributions at low T. If we also take into account the susceptibility of the Cr($4f_{vi}$)-Cr($4f_{vi}$) isolated spin pairs (χ_{pair}), χ_{macro} may therefore be expressed as the sum of three contributions:

$$\chi_{macro}=\chi_{frustr}+\chi_{pair}+\chi_{def}. \tag{1}$$

The dominant Curie susceptibility of the defects, χ_{def}, at low T prevents to probe χ_{frustr} through macroscopic measurements.

Using Eq. (1), we can fit the T dependence of χ_{macro} given some simple remarks and minor assumptions. The T dependence of χ_{frustr} is known through K, and for this reason the fit was performed in the 15 K$\leqslant T \leqslant$350 K range, where we have a full intensity in the NMR signal. This T range of the fit leads to an inaccuracy in the determination of a possible low-T Curie-Weiss temperature of χ_{macro}; hence we assume a pure Curie component $\chi_{def}=C_{def}/T$ to fit the low-T upturn. The susceptibility χ_{pair} is quantitatively derived analytically (see the Appendix). The only unknown parameters of Eq. (1) are the effective moments $\mu_{eff}(4f_{vi})$ of the Cr^{3+} ions of χ_{pair}, the Curie constant C_{def} of the defects, and the hyperfine constant $\mathcal{A}$.

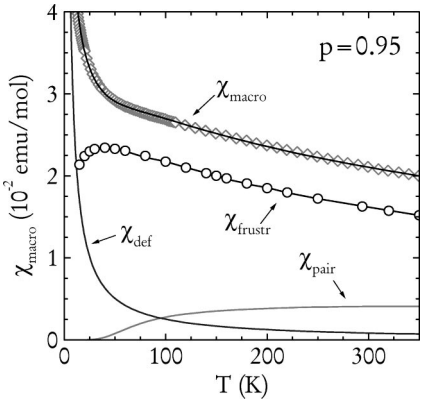

FIG. 13. The three contributions to χ_{macro} obtained through the fit described in the text: the kagomé bilayer susceptibility (χ_{frustr}), the Cr($4f_{vi}$)-Cr($4f_{vi}$) spin-pair susceptibility (χ_{pair}), and the Curie susceptibility induced by dilution ($\chi_{def}=C_{def}/T$).

The fit to χ_{macro} for the $p=0.95$ sample is presented in Fig. 13 and reproduces correctly the evolution of the experimental macroscopic susceptibility in the $T>15$ K range. In Table IV we have reported the fitting parameters extracted from the three samples $p=0.81$,0.89,0.95. The effective moment is close to the 3.87 μ_B value expected for a Cr^{3+} ion, and the Curie contribution C_{def} is found to decrease with increasing p. The values of C_{def} presented here, even if extracted from a fit that does not cover the 5 K$\leqslant T \leqslant$15 K range where χ_{def} dominates, nevertheless are in good agreement with those of Table V, where the C_{def} value is dominantly determined by the very low-T region fit of χ_{macro} (Sec. VI). Finally, $\mathcal{A}$ is nearly constant with p, confirming the assumption of Sec. II that the site dilution does not alter in a significant way the couplings in SCGO, hence that the Ga-O-Cr hyperfine interaction is also constant with the dilution.

C. Discussion

We compare here our experimental data for the intrinsic susceptibility χ_{frustr} of the frustrated lattice reflected in K to the calculations performed for the kagomé and the pyrochlore networks through different approaches.

Within a classical frame where the minimization of the Heisenberg Hamiltonian is constructed on the basis of nonmagnetic triangles and tetrahedras, different authors have simulated the susceptibility of the kagomé and the pyrochlore network by Monte Carlo calculations.[31,46,47] All these models suggest a Curie-Weiss susceptibility, which extends to low T ($T \ll \Theta$), in agreement with the high-T behavior of K ($T>100$ K). Although these models do not predict a

TABLE IV. The fitting parameters $\mu_{eff}(4f_{vi})$, C_{def}, and $\mathcal{A}$ for the $p=0.81$,0.89,0.95 samples used to reproduce χ_{macro} by Eq. (1).

p	$\mu_{eff}(4f_{vi})$	C_{def} (emu K/mol)	$\mathcal{A}\times 10^3$ (Oe/μ_B)
0.81	4.0(6)μ_B	0.51(12)	3.4(4)
0.89	4.5(4)μ_B	0.45(10)	3.8(4)
0.95	4.3(2)μ_B	0.25(5)	3.9(2)

TABLE V. The parameters of the two-component fit to χ_{macro} described in the text. At low dilution, the fit yields a stronger error.

p	C (emu K/mol)	Θ (K)	C_{def} (emu K/mol)	Θ_{def} (K)	C_{def}/C (%)
0.72	14.0(2)	467(19)	0.53(3)	2.3(1.0)	3.8(2)
0.81	17.6(3)	650(15)	0.39(3)	0.9(1.0)	2.2(2)
0.89	20.5(4)	752(17)	0.34(3)	0.6(1.0)	1.7(2)
0.90	22.0(6)	792(25)	0.24(3)	0.5(2.0)	1.0(2)
0.95	23.5(7)	826(22)	0.15(3)	0.2(2.0)	0.6(2)

maximum in the susceptibility versus temperature, all agree with our results on the absence of a Curie upturn at low T as is detected in χ_{macro}.

The susceptibility for the $S=1/2$ kagomé network has been calculated by an exact diagonalization of the Heisenberg Hamiltonian.[11] As mentioned in the Introduction, the ground state is constructed here on nonmagnetic spin singlets and a "gap" (Δ) is predicted between the singlet ground state and the magnetic spin triplet state. The calculated susceptibility hence varies as $\sim\exp(-\Delta/T)$ at low T, with a maximum in the susceptibility occurring at $\Delta\approx 0.1J$. However, it seems difficult to reconcile this maximum with our results. First, we would expect to observe in K a much sharper decrease in temperature than what is observed experimentally. Second, the energy scale of Δ itself does not agree with our data. In fact, taking $J\approx 80$ K, the maximum of K falls at $T_{max}\approx 0.5J>\Delta$ (note that Δ should be weaker than $0.1J$ for $S=3/2$ spins or even disappear).[48] The interpretation of the observed maximum for SCGO has to be researched elsewhere than in the gap predicted by this model. We stress that the Ga($4f$) NMR intensity loss does not allow us to probe deeply the predictions of this model, which places the gap in the $T<15$ K range. But, clearly, our data reveal that other parameters have to be taken into account for $T\gg\Delta$ to explain the origin of the maximum in K vs T at $\approx 0.1\Theta$.

In this context, it appears natural to seek an interpretation in more conventional terms. The maximum in K versus temperature indicates an increasing magnetic rigidity of the kagomé bilayer spin network. As in all the $d=2$ AF systems, we suggest that the maximum is an experimental signature of a small reinforcement of the magnetic correlations. The quasiconstancy of K for all p below this maximum (only a slight decrease is observed) is, therefore, an indication that the correlations are short ranged and concomitantly do not depend on the dilution.

Let us recall the typical characteristics evidenced in the susceptibility of $d=2$ AF networks with Heisenberg spins as reviewed in Ref. 49. At high T, the $d=2$ susceptibility follows a Curie-Weiss law, but exhibits a maximum in the susceptibility at a temperature $T_{max}\approx\Theta$, which is a consequence of the development of magnetic correlations. However, in contrast with $d=3$ systems where a long-range order is established at $T_c\approx\Theta$, a $d=2$ system has a finite correlation length at $T_{max}\approx\Theta$ that eventually diverges when $T\rightarrow 0$ K. The low dimensionality of the lattice inhibits the full development of the critical fluctuations. In the case of the kagomé bilayer of SCGO, we suggest that the geometric frustration is even more efficient in preventing correlations to develop, moving the maximum in χ_{frustr} down to $T_{max}\approx 0.1\Theta$.

On the experimental side, neutron-diffraction measurements further support this point of view. As mentioned in Sec. I, neutron studies on SCGO have established that the magnetic correlations in the SG phase ($T<T_g$) are short ranged. Mondelli *et al.* observed recently the neutron-diffraction spectrum in a wider temperature range than the previous experiments (1.5 K$\leqslant T\leqslant$200 K).[50] As shown in Ref. 50, the characteristic diffuse peak typical for short-range correlations ($\xi\approx 2\times d_{\text{Cr-Cr}}$) develops at $T\leqslant 60$ K, precisely in the same temperature range where the maximum in χ_{frustr} occurs. This maximum is, therefore, the signature in the susceptibility of the development of these short-range correlations. The feeble decrease in χ_{frustr} we observe simply reflects the finite value of ξ at $T<T_{max}$.

A recent quantum mean-field theory study also points at this direction.[51] The basic idea here is to explicitly account for the magnetic correlations by constructing the ground state not on interacting spins, but on interacting triangles or tetrahedras of spins. Within this framework, García-Adeva and Huber calculated the susceptibility of the kagomé and the pyrochlore networks for various spin values, providing a reference for comparisons to our Ga NMR shift K (their mean-field theory does not account for the existence of a spatially nonuniform susceptibility responsible for the NMR linewidth broadening, see Sec. VI). In a recent paper,[52] they also studied the influence of the lattice dilution on the susceptibility of these networks. This theory seems to capture most of the main features of our data: the calculated susceptibility for the diluted kagomé and pyrochlore networks exhibits a maximum at $T_{max}\sim 0.15\Theta$ followed by a feeble decrease of the susceptibility in the 0.05Θ–0.15Θ temperature range. Although the order of magnitudes found are very encouraging, as we underline in the bottom panel of Fig. 11, more experimental and theoretical studies are needed here to completely validate this model. Indeed, García-Adeva and Huber predict that the susceptibility's maximum should be progressively washed out with increasing dilution and eventually disappear (for a dilution of $\sim$10–15 % in a $S=5/2$ kagomé lattice and for a dilution of $\sim$20–30 % in a $S=3/2$ pyrochlore lattice), a feature that somewhat contradicts our observations. Furthermore, as evidenced in the bottom panel of Fig. 11, the T dependence of K for $T>T_{max}$ is dilution independent. This would only agree with the susceptibility calculated for a diluted pyrochlore lattice, but for $T<T_{max}$ the more pronounced decrease in K we observe is opposite

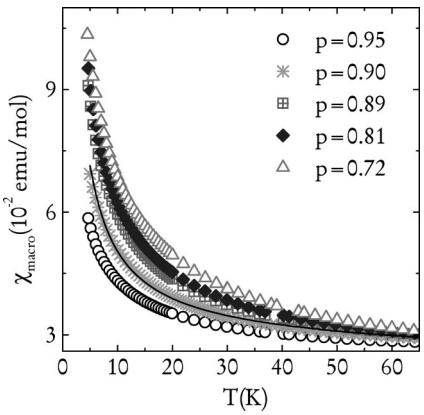

FIG. 14. The low-T macroscopic susceptibility of some of the SCGO samples studied. The solid line is the two-component fit [Eq. (2)] to the $p=0.90$ sample.

to what is predicted for the pyrochlore lattice. Unfortunately the Ga NMR intensity loss at $T<15$ K (Sec. IV A) does not enable us to further verify their model, in particular, to verify whether there is a Curie-like upturn in the susceptibility for $T \ll 0.05\Theta$. We conclude then that for an adequate comparison between data and theory, the influence of the kagomé bilayer structure should be taken into account in the calculations. Also, the nonrandom distribution of the nonmagnetic vacancies in SCGO's kagomé bilayer might induce quantitative differences between the calculated and experimental susceptibilities, as pointed out in Ref. 52.

The general picture drawn by our overview of the experimental and theoretical data is that even short-range spin-spin correlations clearly play a major role in SCGO, or more generally in all geometrically frustrated compounds. Future studies are required in this direction to further uncover the low-T properties of these systems.

VI. DILUTION EFFECTS

In this section, we focus on the dilution-dependent susceptibility revealed by the NMR linewidth at low T. We show that the low-T paramagnetic behavior observed in χ_{macro} originates from the dilution of the kagomé bilayer. This feature is observed in nearly all the geometrically frustrated AF compounds and appears as a generic behavior of this class of materials.[31]

Naturally, the macroscopic susceptibility could allow, in some way, to appreciate the dilution effects through its low T behavior. Though, the multiplicity of the Cr sites in SCGO complicates the analysis. The Ga($4f$) NMR width not only enables to evidence that the vacancy of a spin on the network, i.e., the dilution, generates a paramagnetic defect, but also allows to shed light on the more fundamental question concerning the nature of the defect.

A. Low-T macroscopic susceptibility

In Fig. 14 we present the low-T macroscopic susceptibility of most of the samples studied. The low-T paramagnetic upturn of χ_{macro} is observed at all the concentrations, increasing in an appreciable way with growing dilution. This establishes that the origin of this contribution is related to the Ga/Cr substitution. The nonmagnetic gallium vacancy on the network must, therefore, induce a perturbation, which affects the neighboring magnetic Cr^{3+} ions. A paramagnetic defect is then generated, whose susceptibility χ_{def} is reflected in the low-T behavior of χ_{macro}.

In order to determine the exact low-T dependence of the susceptibility associated with the defects, the contribution to χ_{macro} of both χ_{frustr} and χ_{pair} should, in principle, not be neglected. Since χ_{frustr} cannot be determined through NMR below 15 K, we follow Ref. 31 and conveniently fit χ_{macro} by a two-component expression

$$\chi_{macro}=\frac{C}{T+\Theta}+\frac{C_{def}}{T+\Theta_{def}}. \tag{2}$$

Anyhow, the corrections from χ_{frustr} and χ_{pair} are small at low T compared to χ_{def} and do not affect significantly the analysis. The first Curie-Weiss term roughly takes into account the contribution from χ_{frustr} and χ_{pair}, which dominate at high T. The second term, the more relevant for this section, also Curie-Weiss, quantifies the contribution of χ_{def}.

The fits, shown by a solid line in Fig. 14 for the $p=0.90$ sample, were performed in the 5 K$\leqslant T \leqslant$350 K range for all the samples and reproduce correctly the low-T behavior of χ_{macro}. The fitting parameters are presented in Table V and are in agreement with Ref. 31. The values of C and Θ yield an overestimate of $\approx$10–20 % compared to those of Table I. The values of C_{def} are in agreement with the analysis of Sec. V. As expected, C_{def} decreases with the dilution and most importantly is found to be only a weak fraction of the constant C, $C_{def}/C \sim 1\%$ (Table V). Finally, the Curie-Weiss temperature Θ_{def}, which is an indication of the average interaction between the defects, is negligibly small within error bars except for the $p=0.72$ sample for which it is at most 2 K.

Strictly speaking, it should be finally noticed that χ_{macro} is not sufficient on its own to establish experimentally whether the defects stem from the dilution of the kagomé bilayer. Indeed, the Ga/Cr substitution on a Cr($4f_{vi}$) site can, in principle, break a spin pair and free a paramagnetic spin, which can then contribute to the paramagnetic upturn of χ_{macro}. In contrast with χ_{macro}, Ga($4f$) NMR is not sensitive to Cr($4f_{vi}$) and, as presented in the following section, allows a better understanding of the dilution effects in SCGO.

B. Dilution effects through the Ga($4f$) NMR width

In Fig. 15 we present the T dependence (10 K$\leqslant T \leqslant$60 K) of the low-T width of ^{69,71}Ga($4f$) ($^{69,71}\Delta H$) for five of the seven samples studied. We recover here the properties mentioned about the raw spectra: $^{69,71}\Delta H$ increases as the temperature drops and is very sensitive to the dilution, in contrast with K. The low-T behavior of $^{69,71}\Delta H$ bears strong similarities to that of χ_{macro}. The perfect scaling of the widths of the two isotopes, $^{69,71}\Delta H$, normalized by the ref-

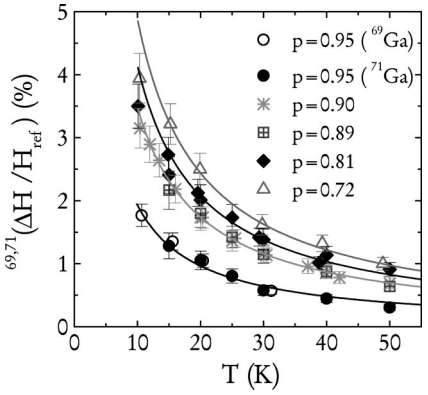

FIG. 15. $^{69,71}\Delta H$ versus T for some samples studied. $^{69,71}\Delta H$ is extracted from the $\nu_{rf}=40.454$ MHz spectra following the fit described in Sec. IV B. $^{69,71}\Delta H$ is normalized by the reference field $^{69,71}H_{ref}$ to superimpose results from the two isotopes (as explicitly shown for $p=0.95$). The solid lines are the Curie-Weiss fits $C_{def/NMR}/(T+\Theta_{def/NMR})$.

erence field $^{69,71}H_{ref}$ $(=\nu_{rf}/^{69,71}\gamma)$—explicitly shown for the $p=0.95$ sample in Fig. 15—underlines the magnetic origin of the low-T broadening ($^{69,71}\Delta H\propto{}^{69,71}H_{ref}$), in agreement with the prior study on the $p=0.90$ sample.[32]

The fact that the ^{69,71}Ga$(4f)$ linewidth increases rapidly at low T and with the dilution, whereas the shift varies little, establishes the existence of a susceptibility that is *spatially inhomogeneous* over the kagomé bilayer, due to the defects associated with the Ga/Cr substitution. Since the Ga$(4f)$ nuclei are only coupled to the kagomé bilayer, the *defects* probed by Ga NMR are necessarily *localized in the kagomé bilayer*.

The effect associated with the dilution is not reduced to a mere suppression of a Cr site without any magnetic signature over the neighboring spins (i.e., a magnetic defect) as indicated by the large modification of the ^{69,71}Ga$(4f)$ line shape at low T. Indeed, in the opposite case, one would expect a line shape, which results from the gallium nuclear spins coupled to various Cr environments all bearing the same susceptibility. One would, therefore, expect the linewidth to scale with the susceptibility, then K, which varies only by 20% from 60 K to 15 K, whereas the linewidth increases by one order of magnitude. For this very same reason, a spatial distribution of the hyperfine constant, which yields also a width proportional to K, cannot justify the broadening observed and also has to be ruled out.

The T dependence of $^{69,71}\Delta H$ is correctly reproduced by a Curie-Weiss law of the form $C_{def/NMR}/(T+\Theta_{def/NMR})$, where $C_{def/NMR}$ is a constant and $\Theta_{def/NMR}$ a Curie-Weiss temperature. The fits are presented in Fig. 15 as solid lines. The values of $\Theta_{def/NMR}$ are extremely low, with a maximum of ≈ 4 K, and vary *randomly* with dilution. Although we cannot exclude completely a Curie-Weiss behavior, especially at high dilution, we may consider the evolution in temperature of $^{69,71}\Delta H$ as very close to a Curie law. The values of $C_{def/NMR}$ are plotted as a function of $(1-p)$ in the top panel of Fig. 16 (right y axis) along with the values of

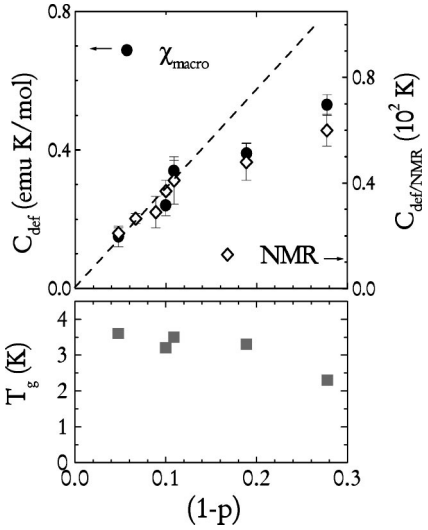

FIG. 16. Top panel: C_{def} extracted from χ_{macro} (left) and $C_{def/NMR}$ (right) extracted from the NMR width $^{69,71}\Delta H$ versus dilution $(1-p)$. The dashed line is a guide to the eye. Bottom panel: The SG temperature T_g of our SCGO samples versus dilution.

C_{def} extracted from χ_{macro} by Eq. (2) (left y axis).[53] As shown, the dependencies of both C_{def} and $C_{def/NMR}$ on $(1-p)$ perfectly match, suggesting that $^{69,71}\Delta H$ and χ_{macro} probe the same susceptibility at low T, i.e., χ_{def}. This is further underlined in Fig. 17 by the linear relationship between $^{69,71}\Delta H/H_{ref}$ and χ_{macro} at low T. Since the defects probed by Ga NMR are located in the kagomé bilayer, Figs. 16 and 17 indicate that the defects on the Cr$(4f_{vi})$ sites yield a contribution scaling with that one from the kagomé bilayer or contribute little to χ_{macro}. In view of the quantitative analysis of C_{def} presented in Ref. 54, the latter explanation is the more plausible. Finally, we note in Fig. 16 that $C_{def/NMR}$ and C_{def} are linear with $(1-p)$ at low dilutions ($p>0.90$), and become progressively sublinear with $(1-p)$ at higher dilutions. This deviation is directly perceptible in the spectra of Fig. 9, where the full width at half maximum of the $p=0.81$ sample is clearly not four times that of the $p=0.95$ sample.

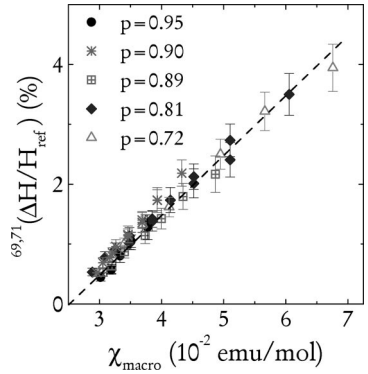

FIG. 17. $^{69,71}\Delta H$ versus χ_{macro} for some of the samples studied (T is an implicit parameter).

C. Discussion on the nature of the defect

1. Models for the localized defects

To our knowledge, two models describe the dilution effects in a geometrically frustrated system. Both are constructed in a classical approach where the ground state corresponds to a minimization of the exchange energies on triangles (or tetrahedras) of spins.

The most recent model was proposed by Moessner and Berlinsky.[47] The basic idea here is that a paramagnetic moment in the kagomé network is generated when two vacancies are adjacent on a triangle (three adjacent vacancies are needed for the pyrochlore network). The defect corresponds in this case to a unique spin of the network, and at low dilution the defect's susceptibility is $\chi_{def} \sim (1-p)^2/T$ for the kagomé network [$\sim(1-p)^3/T$ for the pyrochlore network]. This prediction is in striking contrast with the linear variation of the NMR width on dilution reported in Fig. 16. To reconcile our data to the theory of Ref. 47, it was suggested in Ref. 55 that the magnetic broadening of the width may reflect a distribution of random local fields ($\propto \chi_{def}$) due to the coupling of each gallium nucleus to the 12 neighboring Cr sites of the kagomé bilayer. Basically, the NMR width ΔH would then probe the mean deviation of the susceptibility on these 12 sites (and not simply χ_{def}), thus $\Delta H \propto \sqrt{(1-p)^2/T}$. Although appealing, this scenario is quite unlikely since the macroscopic susceptibility measurements, which are insensitive to the effect of a local summation of fields, do not yield a quadratic $(1-p)^2$ variation on dilution.

The second model—purely empirical—was proposed in Ref. 31. There, a defect is generated by a vacancy, which perturbs the neighboring spins, uncorrelating them from the rest of the spin network. These uncorrelated spins were baptized ''orphan'' spins. Two distinct spin populations then coexist: the orphan spins with a paramagnetic behavior making up the defect and the frustrated spins outside the defect with a susceptibility equal to χ_{frustr}. In order to examine the implications of the orphan model on the Ga($4f$) NMR low-T spectrum, we assume, as a starting point, that the defect is built only on the orphan spins that are nearest neighbors (nn) of the vacancy (Fig. 18). We consider the important case of the $p=0.95$ sample where the dilution is weak enough to allow refined conclusions and where the Ga/Cr substitution occurs only on the kagomé layers [the Cr($2a$) site is not substituted, see Fig. 3]. A simulation allows us to model the expected line shape. To do so, we start by randomly suppressing 5% of the spins on the kagomé network to account for the existence of nonmagnetic vacancies. The nn spins of the vacancies are given a susceptibility $\propto \mu_{eff}^2(def)/T$, where $\mu_{eff}(def) \approx 1.5\mu_B$ (evaluated later in the section) to account for the orphan spins, whereas the remaining Cr sites are given a susceptibility χ_{frustr}. Next, we classify the various nuclear populations along their Cr environments. To construct the spectrum, each population is associated to a quadrupole line simulated with the parameters of Table II, with a shift reflecting their Cr environment and an intensity weighted by the population size. Finally, the Ga($4f$) NMR simulated line is obtained by summing the spectra associated with all the nuclear populations. The line simulation for $T=20$ K and $T=10$ K is presented in Fig. 18. As shown, neither the broadening, nor the simulated line shape agree with our ^{71}Ga($4f$) low-T experimental spectrum. Indeed, in the $p=0.95$ sample, $\approx$35% of the gallium nuclei do not probe an orphan spin, hence $\approx$35% of the spectral weight yields a shift proportional to χ_{frustr} (short dashed line in Fig. 18). The majority of the gallium nuclei probe at least one orphan spin, so that $\approx$65% of the spectral weight yields a shift dominated by a $1/T$ contribution at low T (dashed line in Fig. 18). *Independently of the value of* μ_{eff}, one would, therefore, expect to observe $\approx$65% of the spectral weight to shift toward the low fields with decreasing temperature whereas the remaining part is shifted little. This would yield a nonobserved asymmetric broadening of the NMR line with decreasing temperature.

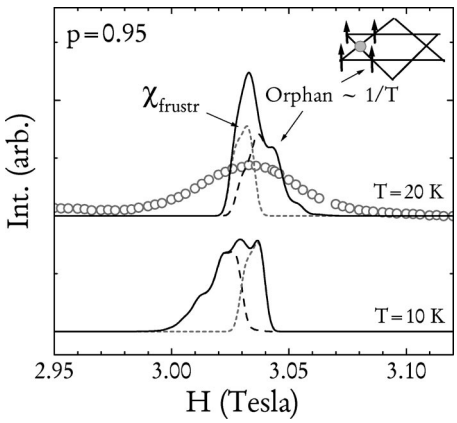

FIG. 18. The simulated sweep field central line of ^{71}Ga($4f$) at $T=20$ K and $T=10$ K ($\nu_{rf}=40.454$ MHz) if orphan spin nn to the vacancy were present in the kagomé bilayer of the $p=0.95$ sample. Also shown is the experimental central line of ^{71}Ga($4f$) recorded for $p=0.95$ at 20 K (open circles). The area of the experimental and of the simulated lines are normalized.

Clearly, a model built on orphan spin nn of the vacancy is unsatisfactory and the perturbation generated by the vacancy must be extended in space. Can we then imagine the defect to be made up of orphan spins that are first, second, third, etc. neighbors of the vacancy? Since the spin-spin interaction is AF this situation is very unlikely to occur.[56] As we show below, an extended staggered perturbation constructed on an AF interaction is conceivable.

2. A defect built on AF correlations

In Sec. V we showed via the observed NMR shift that χ_{frustr} exhibits a maximum in temperature, a common feature for the AF correlated systems. It is, therefore, natural to seek an interpretation for the origin of the paramagnetic defect also in the general context of the AF correlated systems. Indeed in the AF systems such as the $d=1$ spin chains,[57] the quasi-two-dimensional spin ladders,[58] and the $d=2$ cuprates,[59] it is now well established that a vacancy (or a magnetic impurity) generates a long-range oscillating magnetic perturbation and creates a paramagnetic component in the macroscopic susceptibility. The *symmetric* broadening of the NMR line observed in these systems is to be related to

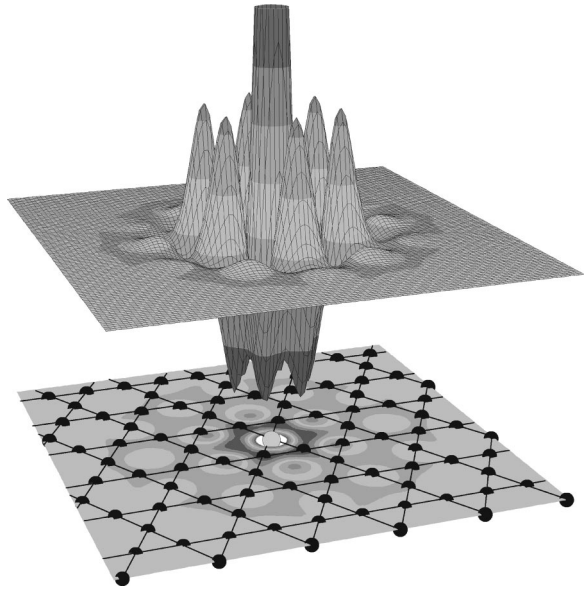

FIG. 19. A Gaussian staggered polarization of arbitrary intensity generated by a vacancy (center of the figure) on a 50-site kagomé lattice. ξ is twice the spin-spin distance and the staggered vector is $\vec{Q}=(1/3,1/3)$, i.e., the vector of the $\sqrt{3}\times\sqrt{3}$ kagomé spin configuration.

the *oscillating* character of the perturbation. We propose that the dilution effects of the SCGO kagomé bilayer can be described by the same physics of these correlated systems.

We recall first some basics concerning this model. The presence of a vacancy in the AF correlated network of spins develops a magnetic perturbation, which, in a general fashion, affects a spin at the lattice position $\vec{r}$ as

$$m(\vec{r})\sim\chi'(\vec{r})H_{ref},$$

where $m(\vec{r})$, $\chi'(\vec{r})$, and H_{ref} are the magnetization, the susceptibility, and the applied magnetic field (constant over $\vec{r}$). For an AF system, $\chi'(\vec{r})$ is peaked at a given vector $\vec{Q}$. As an example, we choose $\chi'(\vec{r})$ to have a Gaussian shape

$$\chi'(\vec{r})=\chi^*\mathcal{G}(\vec{r}\cdot\vec{Q})\exp(-r^2/4\xi^2),$$

where the function $\mathcal{G}(\vec{r}\cdot\vec{Q})$ is oscillating and periodic in $\vec{r}$ with a periodicity related to $\vec{Q}$. ξ is the spin-spin correlation length and χ^* is the amplitude of $\chi'(\vec{r})$. This translates into an oscillating polarization of the spin network with a periodicity of $\sim Q^{-1}$ and damped over $\sim\xi$.

In Fig. 19 we illustrate this with a polarization calculated for the kagomé network. In the absence of low diluted single crystals necessary to determine the exact form of $\chi'(\vec{r})$ and the nature of the vector $\vec{Q}$ through neutron-diffraction experiments, we assume a Gaussian shape for $\chi'(\vec{r})$ and take the reciprocal vector $\vec{Q}=(1/3,1/3)$ of the so-called kagomé $\sqrt{3}\times\sqrt{3}$ spin configuration. By selecting this vector, we partially account for the effects related to frustration.

The staggered shape of the polarization ensures that the NMR line of the nuclei probing the spins of the lattice is broadened on both sides, i.e., that the broadening is symmetric and scales with the applied field, in agreement with our data. *A nonstaggered polarization would generate only local fields pointing in the same direction and the NMR line would then be only broadened on one side, i.e., the broadening would be asymmetric (as in the orphan spin model)*. The actual shape of the broadening (Gaussian, Lorentzian, etc.) depends on $\chi'(\vec{r})$, on the vector $\vec{Q}$, and on the geometrical details of the nucleus-spin coupling.

On the macroscopic stand, the vacancy generates a paramagnetic defect with a macroscopic susceptibility

$$\chi_{def}=\frac{(1-p)\mu_{eff}^{(def)\,2}}{3k_BT}, \tag{3}$$

where $\mu_{eff}^{(def)}$ is the effective moment of a defect. Although the exact nature of the defect is not well established and is still the object of theoretical studies,[60] two scenarios may be conceived.

(1) The defect is the sum of all the polarizations, in other words the magnetization $M=\Sigma_{\vec{r}}m(\vec{r})$, whose susceptibility is paramagnetic. The $1/T$ variation of the overall moment has then no intuitive explanation.

(2) The vacancy generates a localized paramagnetic moment on the nn spins, which generates the staggered response $\chi'(\vec{r})$ in the spin network. In this case, one needs to understand microscopically why a paramagnetic moment is created.

Quantitatively, the expected NMR broadening is magnetic and related to χ^* and ξ by

$$\Delta H\propto\mathcal{A}\chi^*\mathcal{F}(\xi,1-p)\frac{H_{ref}}{T}, \tag{4}$$

where $\mathcal{A}$ is the hyperfine coupling constant between the spin and the nucleus. $\mathcal{F}$ is a function of ξ and of the dilution $(1-p)$. The form of $\mathcal{F}$ depends on the form of $\chi'(\vec{r})$.

The NMR width is sensitive to all variations in T of $\xi(T)$ and $\chi^*(T)$ in contrast with the macroscopic measurements. The surprising simple $1/T$ variation of ΔH we observe by Ga NMR in SCGO might indicate that once the correlations set in below 50 K, very little changes occur for $\xi(T)$ and $\chi^*(T)$ due to the high frustration. Concerning $\xi(T)$, neutron measurements are very rewarding since they do infer that the spin-spin correlation is constant with temperature when $T\leqslant 60$ K (Sec. V).

At low dilution, where the interaction between the defects can be neglected, $\mathcal{F}(1-p)\propto(1-p)$. The evolution of $C_{def/NMR}$ with the dilution reflects that of $\mathcal{F}(\xi,1-p)$. Figure 16 indicates that $C_{def/NMR}$ is linear with $(1-p)$ at low dilution, but deviates progressively from linearity at higher dilution. This deviation is indeed expected. It can be associated with an ''interference'' between the polarizations induced by the nearby vacancies. This phenomenon, known now for several years, was first evidenced in the case of the Ruderman-Kittel-Kosuya-Yosida polarization in the dilute alloys.[61] It is very important to note that $C_{def/NMR}$ likely extrapolates to zero when $p\rightarrow 1$ or in the worst case to a value lower than the observed values of $C_{def/NMR}$ for $p\leqslant 0.95$. Since the SG

state occurs at nearly the same temperature in all the samples and T_g varies in the opposite way of $1-p$ (bottom panel of Fig. 16), this clearly demonstrates that *the origin of the SG state is not related to the dilution-induced defects*. Whether a small residual p-independent Curie term associated with intrinsic (topological) defects might explain the freezing is still a matter of speculation as Cr concentrations higher than $p>0.95$ would be necessary to conclude.

To summarize, our NMR and macroscopic susceptibility results agree perfectly with a picture of a defect built on the AF correlations of the frustrated network. In conclusion we now elaborate on the effective value of the paramagnetic moment detected in the low-T macroscopic susceptibility.

Following Eq. (3) and from the C_{def} constant of Table V, we deduce a nearly p-independent value for the defect effective magnetic moment of $\mu_{eff}^{(def)} \approx 1.5\mu_B$ smaller than the expected $3.87\mu_B$ value for a free $S=3/2$ spin. The weak ratio C_{def}/C of Table V is then simply explained in this viewpoint since $C_{def}/C=(1-p)\mu_{eff}^{(def)\,2}/p\mu_{eff}^2(Cr^{3+}) \approx 0.15(1-p)/p$. We can either speculate that the geometric frustration might diminish the efficiency of the polarization induced by the vacancy, indication that the nature of the defect is complex, or the paramagnetic defect can be modeled into a $S=1/2$ spin quantum state. Also, in the case where $\mu_{eff}^{(def)}$ results from the sum of the oscillating spin polarization, there is no reason to find a 3/2 value. Further theoretical work in this direction is indeed required to model the defect and achieve a quantitative understanding of our data.

VII. SUMMARY AND CONCLUDING REMARKS

The SCGO kagomé bilayer compound was studied through a local probe over a wide variety of Cr concentrations. We unraveled properties of the archetype of geometrically frustrated compounds, otherwise nonaccessible through macroscopic measurements.

Ga($4f$) NMR allowed us to observe the kagomé bilayer susceptibility χ_{frustr}. A maximum in χ_{frustr} occurs at a temperature $T_{max} \approx 0.1\Theta$, robust to a dilution as high as $\approx 20\%$. No gaped feature is evidenced. The maximum signals the appearance of short-ranged magnetic correlations in the kagomé bilayer, as observed in all the AF $d=2$ Heisenberg systems. T_{max} is an energy scale for SCGO, which sets a new constraint on the theoretical models.

A close examination of the dilution effects by Ga($4f$) NMR allowed us to establish, on a firm experimental ground, that paramagnetic defects are present on the kagomé bilayer. The defects stem from the vacancies in the spin network, i.e., from the substitution of magnetic Cr^{3+} ions with nonmagnetic Ga^{3+} ions. The defects are responsible for the low-T Curie upturn of χ_{macro}. The macroscopic susceptibility, therefore, does not probe an intrinsic property of the kagomé bilayer at low T, but mainly a property related to the dilution. Interestingly, the SG transition is detected precisely in the low-T upturn of χ_{macro}. As there are experimental signatures suggesting that this transition is an intrinsic feature of SCGO,[25,62] this means that the defects do not trigger the freezing, but do freeze at $T<T_g$. The origin of the SG transition remains to be elucidated.

Finally, we proposed a mechanism that justifies the existence of the paramagnetic defects, which, to our knowledge, is the only one that gives a consistent interpretation for both the Ga($4f$) NMR and the macroscopic susceptibility results. Our NMR data point at a defect that possesses strong analogies with the defects observed in most of the AF correlated systems—where the presence of a vacancy (or a magnetic impurity) generates a staggered response from the spin network. Up to now, the dilution in SCGO, or more generally in the frustrated systems, has been considered as a parasitical effect to be minimized in order to measure the intrinsic properties related to the geometric frustration. In light of our results, it is interesting to adopt another point of view. The study of the response from the magnetic lattice to a nonmagnetic vacancy can be an indirect way of probing the intrinsic properties of the frustrated network such as $\xi(T)$ or $\chi^*(T)$. The experimental study and the theoretical models to describe this response are a yet undiscovered domain of investigation for the geometrically frustrated systems.

ACKNOWLEDGMENTS

It is a pleasure to thank J. Bobroff, H. Alloul, A. Keren, C. Lhuillier, and F. Mila for fruitful discussions.

APPENDIX: SUSCEPTIBILITY OF AN ISOLATED SPIN PAIR

We consider pairs of spins s with an AF exchange constant J. Their states are labeled by their total spin quantum number $S=0,1,2,\ldots,2s$, and lie at energies $E_S=JS(S+1)/2$ relative to the ground state. The partition function for N independent pairs ($2N$ being the total number of spins involved in pair formation) is

$$\mathcal{Z}=\left[\sum_{S=0,2s} g_S \exp(-\beta E_S)\right]^N,$$

where g_S is the degeneracy of each level and $\beta=1/k_BT$. The sum is taken over $S=0,1,2,3,\ldots,2s$. We now apply an external field H to calculate the susceptibility. The degeneracy is lifted by a Zeeman splitting $E_{m_S}(H)=g\mu_B H m_S$ so that

$$\mathcal{Z}(H)=\left[\sum_{S=0,2s}\ \sum_{m_S=-S,S} \exp[-\beta(E_S+E_{m_S})]\right]^N,$$

where $m_S=-2s,\ldots,0,\ldots,2s$ are the Zeeman levels for a spin S. From the expression of $\mathcal{Z}(H)$ we then derive the susceptibility of N isolated spin pairs

$$\chi=\frac{Ng^2\mu_B^2}{k_BT}\frac{\sum_{S=0,2s}\ \sum_{m_S=-S,S} m_S^2 \exp(-\beta E_S)}{\sum_{S=0,2s} g_S \exp(-\beta E_S)}.$$

The susceptibility of a $Cr(4f_{vi})$-$Cr(4f_{vi})$ spin pair ($s=3/2$) per formula unit of SCGO is, therefore,

$$\chi_{pair} = p_{4f_{vi}}^2 \frac{\chi}{N} = \frac{p_{4f_{vi}}^2 \mu_{eff}^2}{s(s+1)k_B T} \times \frac{2\exp(-\beta J) + 10\exp(-3\beta J) + 28\exp(-6\beta J)}{1 + 3\exp(-\beta J) + 5\exp(-3\beta J) + 7\exp(-6\beta J)},$$

where we have introduced the effective moment $\mu_{eff} = \sqrt{g^2 \mu_B^2 s(s+1)}$. The value of the AF exchange constant, i.e., of the singlet-triplet gap, is $J = 18.6(1)$ meV.[33] To account for the dilution effects, χ_{pair} is weighted by $p_{4f_{vi}}^2$, the statistical probability of having a pair of $Cr(4f_{vi})$-$Cr(4f_{vi})$ per formula unit of SCGO. The value of $p_{4f_{vi}}$ is known from neutron refinements (Fig. 3). Note that in the limit $T \gg J/k_B$, we recover the sum of two $s=3/2$ paramagnetic susceptibilities: $2p_{4f_{vi}}^2 \mu_{eff}^2 / 3k_B T$.

*Present address: Institut für Experimentelle und Angewandte Physik, Christian-Albrechts-Universität zu Kiel, D-24098 Kiel, Germany.

[1] R. Liebmann, *Statistical Mechanics of Periodic Frustrated Ising Systems* (Springer-Verlag, Berlin, 1986).

[2] V. Elser, Phys. Rev. Lett. **62**, 2405 (1989).

[3] E. F. Schender and P. C. Holdsworth, *Fluctuations and Order: The New Synthesis* (Springer-Verlag, Berlin, 1994).

[4] I. Ritchey, P. Chandra, and P. Coleman, Phys. Rev. B **47**, 15 342 (1993).

[5] J.T. Chalker, P.C.W. Holdsworth, and E.F. Shender, Phys. Rev. Lett. **68**, 855 (1992); P.W. Leung and V. Elser, Phys. Rev. B **47**, 5459 (1993); C. Zeng and V. Elser, *ibid.* **51**, 8318 (1995).

[6] A. Keren, Phys. Rev. Lett. **72**, 3254 (1994); R. Moessner and J.T. Chalker, Phys. Rev. B **58**, 12 049 (1998).

[7] P.W. Anderson, Mater. Res. Bull. **8**, 153 (1973).

[8] C. Zeng and V. Elser, Phys. Rev. B **42**, 8436 (1990); N. Elstner and A.P. Young, *ibid.* **50**, 6871 (1994); F. Mila, Phys. Rev. Lett. **81**, 2356 (1998).

[9] C. Waldtmann, H.-U. Everts, B. Bernu, C. Lhuillier, P. Sindzingre, P. Lecheminant, and L. Pierre, Eur. Phys. J. B **2**, 501 (1998).

[10] B. Canals and C. Lacroix, Phys. Rev. Lett. **80**, 2933 (1998).

[11] P. Sindzingre, G. Misguich, C. Lhuillier, B. Bernu, L. Pierre, Ch. Waldtmann, and H.-U. Everts, Phys. Rev. Lett. **84**, 2953 (2000).

[12] X. Obradors, A. Labarta, A. Isalgue, J. Tejada, J. Rodriguez, and M. Pernet, Solid State Commun. **65**, 189 (1988).

[13] For reviews, A.P. Ramirez, Annu. Rev. Mater. Sci. **24**, 453 (1994); M.J. Harris and M.P. Zinkin, Mod. Phys. Lett. B **10**, 417 (1996); P. Schiffer and A.P. Ramirez, Comments Condens. Matter Phys. **18**, 21 (1996).

[14] *Proceedings of the Highly Frustrated Magnetism Conference 2000*, Waterloo, 2000, edited by M.J.P. Gingras [Can. J. Phys. **79** (2001)].

[15] B.D. Gaulin, J.N. Reimers, T.E. Mason, J.E. Greedan, and Z. Tun, Phys. Rev. Lett. **69**, 3244 (1992); M.J.P. Gingras, C.V. Stager, N.P. Raju, B.D. Gaulin, and J.E. Greedan, *ibid.* **78**, 947 (1997); A.S. Wills, A. Harrison, C. Ritter, and R.I. Smith, Phys. Rev. B **61**, 6156 (2000).

[16] M.J. Harris, S.T. Bramwell, D.F. McMorrow, T. Zeiske, and K.W. Godfrey, Phys. Rev. Lett. **79**, 2554 (1997); A.P. Ramirez, A. Hayashi, R.J. Cava, R. Siddharthan, and B.S. Shastry, Nature (London) **399**, 333 (1999).

[17] J. Villain, Z. Phys. B **33**, 31 (1979).

[18] E.F. Shender, V.B. Cherepanov, P.C.W. Holdsworth, and A.J. Berlinsky, Phys. Rev. Lett. **70**, 3812 (1993).

[19] J.N. Reimers, A.J. Berlinsky, and A.-C. Shi, Phys. Rev. B **43**, 865 (1991).

[20] N.P. Raju, M. Dion, M.J.P. Gingras, T.E. Mason, and J.E. Greedan, Phys. Rev. B **59**, 14 489 (1999); S.E. Palmer and J.T. Chalker, *ibid.* **62**, 488 (2000).

[21] R. Moessner, Phys. Rev. B **57**, R5587 (1998); M.J.P. Gingras, B.C. den Hertog, M. Faucher, J.S. Gardner, S.R. Dunsiger, L.J. Chang, B.D. Gaulin, N.P. Raju, and J.E. Greedan, *ibid.* **62**, 6496 (2000).

[22] M.J. Harris, M.P. Zinkin, Z. Tun, B.M. Wanklyn, and I.P. Swainson, Phys. Rev. Lett. **73**, 189 (1994); J.S. Gardner, S.R. Dunsiger, B.D. Gaulin, M.J.P. Gingras, J.E. Greedan, R.F. Kiefl, M.D. Lumsden, W.A. MacFarlane, N.P. Raju, J.E. Sonier, I. Swainson, and Z. Tun, *ibid.* **82**, 1012 (1999).

[23] A.P. Ramirez, G.P. Espinosa, and A.S. Cooper, Phys. Rev. Lett. **64**, 2070 (1990); P. Schiffer, A.P. Ramirez, K.N. Franklin, and S-W. Cheong, *ibid.* **77**, 2085 (1996).

[24] B. Martinez, F. Sandiumenge, A. Rouco, J. Rodríguez-Carvajal, M. Tovar, M.T. Causa, S. Galí, and X. Obradors, Phys. Rev. B **46**, 10 786 (1992).

[25] B. Martinez, A. Labarta, R. Rodríguez-Solá, and X. Obradors, Phys. Rev. B **50**, 15 779 (1994).

[26] C. Broholm, G. Aeppli, G.P. Espinosa, and A.S. Cooper, Phys. Rev. Lett. **65**, 3173 (1990).

[27] S.-H. Lee, C. Broholm, G. Aeppli, A.P. Ramirez, T.G. Perring, C.J. Carlile, M. Adams, T.J.L. Jones, and B. Hessen, Europhys. Lett. **35**, 127 (1996)

[28] Y.J. Uemura, A. Keren, K. Kojima, L.P. Le, G.M. Luke, W.D. Wu, Y. Ajiro, T. Asano, Y. Kuriyama, M. Mekata, H. Kikuchi, and K. Kakurai, Phys. Rev. Lett. **73**, 3306 (1994).

[29] A. Keren, Y.J. Uemura, G. Luke, P. Mendels, M. Mekata, and T. Asano, Phys. Rev. Lett. **84**, 3450 (2000).

[30] A.P. Ramirez, B. Hessen, and M. Winklemann, Phys. Rev. Lett. **84**, 2957 (2000).

[31] P. Schiffer and I. Daruka, Phys. Rev. B **56**, 13 712 (1997).

[32] P. Mendels, A. Keren, L. Limot, M. Mekata, G. Collin, and M. Horvatić, Phys. Rev. Lett. **85**, 3496 (2000).

[33] S.-H. Lee, C. Broholm, G. Aeppli, T.G. Perring, B. Hessen, and A. Taylor, Phys. Rev. Lett. **76**, 4424 (1996).

[34] H. Ohta H., M. Sumikawa, M. Motokawa, and H. Nagasawa, J. Phys. Soc. Jpn. **65**, 848 (1996).

[35] E.J. Samuelsen, M.T. Hutchings, and G. Shirane, Physica (Amsterdam) **48**, 13 (1970).

[36] C. Mondelli (private communication).

[37] K. Motida and S. Miahara, J. Phys. Soc. Jpn. **33**, 687 (1972).

[38] A. Keren, P. Mendels, M. Horvatić, F. Ferrer, Y.J. Uemura, M. Mekata, and T. Asano, Phys. Rev. B **57**, 10 745 (1998).

[39] J.F. Baugher, P.C. Taylor, T. Oja, and P.J. Bary, J. Chem. Phys. **50**, 4914 (1969).

[40] The contribution of the nonstoichiometric gallium to the ^{69}Ga spectrum is analogous to the ^{71}Ga spectrum. However, ^{69}Ga(sub) is not resolved: the quadrupole effects, more important as compared to the other isotope, enlarge both ^{69}Ga($4f$) and ^{69}Ga(sub) lines and result into two overlapping lines (see Fig. 6).

[41] L. Limot, Ph.D. thesis, Université de Paris-Sud, Orsay, France, 2000.

[42] W.G. Clark, M.E. Hanson, and F. Lefloch, Rev. Sci. Instrum. **66**, 2453 (1995).

[43] Strictly speaking, with this procedure we also convolute the $4e$ line, which stays constant in temperature; however the ^{69,71}Ga($4e$) line is sufficiently large compared to the ^{69,71}Ga($4f$) line so that the convolution has only a negligible effect on the real shape of its spectrum.

[44] Since it is impossible to determine individually $\mathcal{A}_{12k}$ and $\mathcal{A}_{2a}$, respectively, the hyperfine constants of the Ga($4f$)-O-Cr($12k$) and Ga($4f$)-O-Cr($2a$) couplings, we use an average hyperfine constant $\mathcal{A}=(9\mathcal{A}_{12k}+3\mathcal{A}_{2a})/12$. A calculation in Ref. 38 suggests $\mathcal{A}_{2a}/\mathcal{A}_{12k}\approx 2$.

[45] L. Limot, P. Mendels, G. Collin, C. Mondelli, H. Mutka, and N. Blanchard, Can. J. Phys. **79**, 1393 (2001).

[46] A.B. Harris, C. Kallin, and A.J. Berlinsky, Phys. Rev. B **45**, 2899 (1992); J.N. Reimers and A.J. Berlinsky, *ibid.* **48**, 9539 (1993).

[47] R. Moessner and A.J. Berlinsky, Phys. Rev. Lett. **83**, 3293 (1999).

[48] C. Lhuillier (private communication).

[49] L. J. de Jongh, *Magnetic Properties of Layer Transition Metal Compounds* (Kluver Academic, Dordrecht, MA, 1990).

[50] C. Mondelli, K. Andersen, H. Mutka, C. Payen, and B. Frick, Physica B **267-268**, 139 (1999).

[51] A.J. García-Adeva and D.L. Huber, Phys. Rev. Lett. **85**, 4598 (2000); Phys. Rev. B **63**, 174433 (2001).

[52] A.J. García-Adeva and D.L. Huber, Phys. Rev. B **64**, 172403 (2001).

[53] For clarity, we do not take into account the nonrandom character of the Ga/Cr substitution. Since each Ga($4f$) nucleus is coupled to nine Cr($12k$) sites and only to three Cr($2a$) sites, which, moreover, are less substituted than the Cr($12k$) sites, it is safe to use an average p equal to the nominal concentration.

[54] Taking a binomial distribution for Ga/Cr substitutions on the $4f_{vi}$ site, the paramagnetic susceptibility resulting from the broken spin pairs would yield a Curie constant of ≈ 0.36 emu K/mol for the $p=0.95$ sample, more than twice the experimental value of Table V. The substitutions on the $4f_{vi}$ site are, therefore, substoichiometric. Some chemical constraint must favor substitutions by pairs of gallium ions, minimizing the number of paramagnetic spins resulting from the broken spin pairs.

[55] C. Henley, Can. J. Phys. **79**, 1307 (2001).

[56] Furthermore, if this were the case, the gallium nuclei in the highly diluted samples would be only coupled to paramagnetic orphan spins. The gallium line would then shift as $1/T$ at low T, in contrast with our observations.

[57] M. Takigawa, N. Motoyama, H. Eisaki, and S. Uchida, Phys. Rev. B **55**, 14 129 (1997); F. Tedoldi, R. Santachiara, and M. Horvatić, Phys. Rev. Lett. **83**, 412 (1999).

[58] N. Fujiwara, H. Yasuoka, Y. Fujishiro, M. Azuma, and M. Takano, Phys. Rev. Lett. **80**, 604 (1998); S. Ohsugi, Y. Tokunaga, K. Ishida, Y. Kitaoka, M. Azuma, Y. Fujishiro, and M. Takano, Phys. Rev. B **60**, 4181 (1999).

[59] A.V. Mahajan, H. Alloul, G. Collin, and J.F. Marucco, Phys. Rev. Lett. **72**, 3100 (1994); K. Ishida, Y. Kitaoka, K. Yamazoe, K. Asayama, and Y. Yamada, *ibid.* **76**, 531 (1996); J. Bobroff, H. Alloul, Y. Yoshinari, A. Keren, P. Mendels, N. Blanchard, G. Collin, and J.-F. Marucco, *ibid.* **79**, 2117 (1997); P. Mendels, J. Bobroff, G. Collin, H. Alloul, M. Gabay, J.F. Marucco, N. Blanchard, and B. Grenier, Europhys. Lett. **46**, 678 (1999); M.H. Julien, T. Fehér, M. Horvatić, C. Berthier, O.N. Bakharev, P. Ségransan, G. Collin, and J.-F. Marucco, Phys. Rev. Lett. **84**, 3422 (2000).

[60] See, for example, A.W. Sandvik, E. Dagotto, and D.J. Scalapino, Phys. Rev. B **56**, 11 701 (1997).

[61] A.J. Heeger, A.P. Klein, and P. Tu, Phys. Rev. Lett. **17**, 803 (1966); R.E. Walstedt and L.R. Walker, Phys. Rev. B **11**, 3280 (1974).

[62] C. Mondelli, H. Mutka, B. Frick, and C. Payen, Physica B **266**, 104 (1999).